Post-fire Mechanical Properties of Aluminum Alloys and Aluminum Welds

Ryan Douglas Matulich

Thesis submitted to the faculty of the Virginia Polytechnic Institute and State University
in partial fulfillment of the requirements for the degree of

Master of Science
In
Mechanical Engineering

Brian Y. Lattimer
Scott W. Case
Robert L. West

April 22nd, 2011
Blacksburg, VA

Keywords: Aluminum, Welds, Mechanical Properties, Fire, Vickers Hardness

Post-fire Mechanical Properties of Aluminum Alloys and Aluminum Welds

Ryan Douglas Matulich

ABSTRACT

The focus of this research was to quantify the post-fire mechanical properties of 5083-H116 and 6082-T6 aluminum alloys. Post-fire exposure is considered heating the material to a particular temperature then cooling the material back to room temperature. The research included evaluating parent materials as well as welded samples.

Post-fire mechanical properties of parent materials were evaluated at temperatures ranging from ambient to 500^{o}C with isothermal and transient heating. Changes in material properties were evaluated through static tensile tests and hardness testing on cooled samples. Using this data, an assessment was performed to investigate the relationship between hardness and mechanical properties. For the alloys evaluated, empirical relationships were found between Vickers hardness and post-fire strength.

Testing was also performed on butt welded samples of 6082-T6 exposed isothermally to temperatures ranging from ambient to 500^{o}C. Vickers hardness profiles were measured across a sample to quantify the hardness of the weld, heat affected zone, and parent material. This was performed at room temperature and following different heat exposures. Static tensile tests were used to evaluate the effect of reheating on the welded samples. Post-fire strength of welded samples was strongly affected by weld geometry. Parent material hardness varied with reheating while weld hardness remained constant. At select temperatures, this resulted in the weld having a higher Vickers hardness than the parent material. Despite this tensile failure always occurred within the weld.

DEDICATION

This work is dedicated to my family who has supported me and my academic pursuits. To my father who taught me the dedicated work ethic needed to complete my research, my mother who has shown me the importance of never giving up, and my two brothers, Patrick and Jonah, who constantly inspire me to do my best. Also coffee for giving me the power to stay conscious through all of the long hours I worked.

ACKNOWLEDGEMENTS

I would like to acknowledge several people in particular who have enabled me to complete this research:

Brian Y. Lattimer – Thank you for all of the support you have provided as my advisor. Your mentoring during my research has made me a better engineer, and your friendship has made me a better person.

Scott W. Case – Thank you for the critical feedback on materials testing procedures and results. This knowledge was invaluable in the development of my test method and data analysis.

Robert L. West – Thank you for being on my committee and always having an open door.

Patrick T. Summers – Thank you for your support and help in the completion of this research. You were always willing to take time out of your day to help talk me through any part of my project. Your friendship is greatly appreciated.

Craig A. English Jr. – Thank you for being willing to always being there when I needed help with anything. Additional thanks for always providing me with a much needed break from work . Your friendship is greatly appreciated.

Members of the EXTREME Lab – Thank you, especially Jillian Chodak, Emily Fogle, and Thomas Goodrich for their support in and out of the lab. The friendships I have made with everyone is an invaluable asset.

Thank you to all of my friends from my home, my alma mater, and the other labs here at Virginia Tech.

TABLE OF CONTENTS

ABSTRACT ii
DEDICATION iii
ACKNOWLEDGEMENTS iv
TABLE OF CONTENTS v
LIST OF FIGURES vii
LIST OF TABLES ix
1. INTRODUCTION 1
1.1. Motivation 1
1.2. Previous Work 1
1.3. Research Focus 3
2. POST HEATING EFFECTS ON ALUMINUM ALLOYS 4
2.1. Introduction 4
2.2. Experimental 4
2.2.1. Hardness Testing 4
2.2.2. Tensile Testing 5
2.2.3. Heating Methods 6
2.2.4. Materials 8
2.2.5. Testing Overview 9
2.3. Results 10
2.3.1. Post Fire Tensile Tests 10
2.3.2. Hardness 14
2.4. Discussion 17
2.4.1. Effect of Heating on Mechanical Properties 17
2.4.2. Relationship between Mechanical Properties and Hardness 18
2.5. Summary of Findings 19
3. POST HEATING EFFECTS ON WELDS 31
3.1. Introduction 31
3.2. Experimental 31
3.2.1. Tensile Testing 31

3.2.2. Hardness Measurements 33
3.2.3. Heating 34
3.2.4. Material 34
3.3. Results 35
3.3.1. Weld Configuration 1 35
3.3.2. Stress Strain Curves 37
3.3.3. Weld Configuration 2 38
3.3.4. Hardness Measurements 39
3.4. Discussion 42
3.4.1. Effect of Exposure Temperature 42
3.4.2. Relationship of Hardness and Weld Failure Location 43
3.5. Summary of Findings 43
4. CONCLUSIONS 52
REFERENCES 54
APPENDIX 5083 – H116 A 57
APPENDIX 5083 – H116 B 65
APPENDIX 6082 – T651 73
APPENDIX 6082 – T6 EXTRUSION 81
APPENDIX MATERIAL PROPERTIES 89

LIST OF FIGURES

Figure 1 Tensile Testing Results for 5083-H116 A 21

Figure 2 Tensile Test Results for 5083-H116 B 22

Figure 3 Tensile Testing Results for 6082-T651 Plate 22

Figure 4 Tensile Test Results for 6082-T6 Extrusion 23

Figure 5 Modulus of Elasticity of All Test Samples 23

Figure 6 0.2% Yield Stress Results for All Samples 24

Figure 7 Ultimate Tensile Strength 25

Figure 8 Reduction of Area 25

Figure 9 Isothermal Vickers Hardness for (a) 5083-H116 A and (b) 6082-T651 26

Figure 10 Comparison of Vickers Hardness for All Materials at Zero Time 27

Figure 11 Constant Heat Flux Vickers Hardness for (a) 5083-H116 A and (b) 6082-T651 28

Figure 12 Relation of Vickers Hardness to Yield Stress 29

Figure 13 Vickers Hardness Versus Stress at 8% Strain 29

Figure 14 Vickers Hardness Versus Ultimate Tensile Strength 30

Figure 15 Weld Configuration 1[26] 44

Figure 16 Weld Configuration 2[26] 45

Figure 17 Hardness Profiles Across the Different Weld Geometries for (a) Configuration 2 and (b) Configuration 1 45

Figure 18 DIC Calculated Strain Fields for 150^{o}C for (a) initial, (b) onset of yielding, and (c) prior to failure 46

Figure 19 Failure Location of 150°C Weld Sample from Configuration 1 46

Figure 20 DIC Calculated Strain for 300°C Sample for (a) initial, (b) onset of yielding, and (c) prior to failure 46

Figure 21 Break Location for 300°C Sample from Configuration 1 46

Figure 22 DIC Calculated Strain for 400°C for (a) initial, (b) onset of yielding, and (c) prior to failures..... 47

Figure 23 Break Location for 400°C Sample from Configuration 1 47

Figure 24 DIC Calculated Strain for 500°C for (a) initial, (b) onset of yielding, and (c) prior to failure 47

Figure 25 Break Location for 500°C Sample from Configuration 1 47

Figure 26 Tensile Test Results for the Different Geometries for (a) Configuration 2 and (b) Configuration 1 48

Figure 27 Modulus of Elasticity Results..... 49

Figure 28 0.2% Yield Stress Results..... 49

Figure 29 Ultimate Tensile Strength Results 50

Figure 30 Digital Image Correlation Images for 300°C Test Sample Showing Progression of Failure 50

Figure 31 Digital Image Correlation Images For 400°C Sample Showing the Progression of Failure 51

LIST OF TABLES

Table 1 Tensile Test Specimen Gage Dimensions 9

Table 2 Break Locations and Interpolated Hardness Values 51

1. INTRODUCTION

1.1. Motivation

Aluminum alloys are seeing increased usage in construction because of their light-weight and high natural corrosion resistance compared to steel alloys. The melting temperature of aluminum is almost 800^{o}C lower than steel alloys. Aluminum alloys suffer significant losses in mechanical properties when exposed to temperatures below their melting points. Fire exposure is a common cause of exposure to elevated temperatures in structural components. The ability to determine the extent of damage after exposure to elevated temperatures will enhance safety while also lowering repair costs. To do this the properties of aluminum alloys must be evaluated after the materials are exposed to elevated temperatures. The property data could then be related to a non-destructive test, Vickers hardness, to allow assessment of post-fire damage in aluminum structures.

1.2. Previous Work

Significant research has been performed on aluminum structural response at room temperatures. There has been some work conducted on aluminum response during fire. This work has focused on quantifying elevated temperature properties as well as structural response through testing and modeling. Data for normalized yield stress and modulus as temperature increases have been tabulated by Eurocode 9 and the American Society of Metals Handbook [1,2]. The information provided by coding, such as Eurocode 9 and the ASM Handbook, does not account for the permanent change in material properties that occurs in a fire once the material returns to room temperature. Until the annealing temperature or solution heat treating temperature is reached, the codes provide no information on what mechanical properties should

be encountered in post heated samples [3,4]. Maljaars *et al* has modeled and verified the elevated yield stress data by performing tensile tests in several alloys while they are maintained at an elevated temperature [5,6].

Limited characterization data exists on the mechanical properties of aluminum alloys that have been reheated then returned to room temperature, as would a structure that survived a fire. Most understanding on the permanent change in properties as an effect of reheating comes from extrusion processes and attempting to understand welds.

A correlation between Vickers hardness and material strength was explored as a method to assess residual material properties after a fire event. Tabor has discussed at length the physical meaning of indentation hardness testing as the average plastic deformation pressure over the area of the indenter [7]. By assuming that the relationship of material stress with engineering strain is "ideal plastic" (meaning that stress increases linearly with strain until plastic yielding occurs then stress remains near constant as strain increases to failure), an empirical fit of Vickers hardness and material yield stress can be calculated [7-9]. Using shear stress or strain energy criterion to calculate plastic flow, the relationship between indenter pressure and yielding was developed in [8]

$$P \cong 3Y \tag{1}$$

Substituting the equation for Vickers hardness and geometric properties of the pyramidal indenter (area of the base is equal to 92.5% of the surface area) gives an equation in the form [7]

$$Hv \cong 3.3\,Y \tag{2}$$

To verify this relationship for post-fire aluminum samples, the Vickers hardness of aluminum alloys was measured after fire exposure then tensile testing was conducted on the exposed samples to failure.

1.3. Research Focus

The first section of the thesis provides the research performed on the post-fire mechanical response of parent materials. In this aspect of the research, materials were heated isothermally for different periods as well as with constant heat flux for a transient response. Samples were then water quenched to cool back to room temperature. Changes in material properties were evaluated through static tensile tests and hardness testing on cooled samples. Using this data, an assessment was performed to investigate the relationship between hardness and mechanical properties.

The second part of the research focused on extending the testing to butt welded samples of 6082-T6 extrusion. Vickers hardness profiles were measured across a sample to quantify the hardness of the weld, heat affected zone, and parent material. Materials were heated isothermally then water quenched to room temperature. Static tensile tests were used to evaluate the effect of reheating on the welded samples. Recording Vickers hardness profiles in materials exposed to different elevated temperatures provided data on the respective changes in properties of the weld, HAZ, and parent materials.

2. POST HEATING EFFECTS ON ALUMINUM ALLOYS

2.1. Introduction

Aluminum is being utilized in a variety of transportation applications as lightweight replacement for steel structures. Structural integrity of aluminum during and following fire is a significant design consideration due to decreases in aluminum mechanical properties at lower temperatures compared to steel [2]. To date research on response of aluminum in fire has been on properties at elevated temperatures [2] and structural response of components at high temperatures [5,10]. Research has not been performed on the properties of aluminum following a fire. This research focused on measuring the mechanical properties of aluminum specimens following a fire exposure. Materials included in this study were 5083-H116, a work hardened alloy, and 6082-T651, a heat treated alloy. Vickers hardness has been previously related to the yield stress in materials at room temperatures [7,9]. A relationship between post fire mechanical properties and hardness was explored to determine if it could be used for onsite post fire aluminum structures.

2.2. Experimental

A description of the testing methods and equipment used in this study is given in the following paragraphs in this section.

2.2.1. Hardness Testing

Hardness measurements were made using macro Vickers hardness machines. Vickers hardness was used in this work since this measurement has been shown to be directly related to the strength of the material [8]. Measurements were performed using a Leco V-100-A2 bench

top hardness tester and a Krautkramer MIC10-DL portable hardness tester. The portable hardness tester was used in this study to explore the use of this method for field use. All measurements were performed with 5 kgf.

The bench top hardness tester contained a filar optical eyepiece to measure the diagonal length of the square shaped indentations. These diagonal lengths were used to determine hardness by

$$Hv_p = \frac{2*P*\sin\frac{\theta}{2}}{d^2} \quad (3)$$

where P is the applied force in (5 kgf), d is the average diagonal length (mm), and θ is the angle between the faces of the pyramidal indenter (136^o). The average diagonal length was determined by averaging the two measured diagonals of a single indentation.

The portable hardness tester used the ultrasonic contact impedance (UCI) method to electronically determine hardness. Comparison of the methods showed that the UCI method closely adhered to the values obtained from the optically measured indentations; about 6% of variation in the UCI results compared to the optical results. The UCI method required a calibration be performed on a sample similar to that being tested, which was done using a reference block of 5083-H116 aluminum alloy. To keep surface roughness below the limit stated in ASTM A-1038[11], samples were prepared for hardness testing with grade '000' steel wool and rinsed with acetone.

2.2.2. Tensile Testing

Tensile tests were performed in an Instron 4206 test frame equipped with a 150 kN load cell. Tests were performed using displacement control at a rate of 2.54 mm/min to provide consistent test results [12-14] With the samples being extracted from plate material, flat or "dog bone" tensile test samples were machined according to ASTM B-557[15]. Samples used in this

study had overall length of 203.2 mm, width of 25.4 mm, gage length of 50.8 mm, and gage width of 12.7 mm. Sample thicknesses ranged from 4-8 mm depending on the material stock thickness.

Measurements made during experiments included load, cross-head displacement, and sample strain. Sample strain was measured using a MTS 634.12-E54 type extensometer, +/- 50% strain, with a non-linearity of 0.25% and a hysteresis of 0.10%, from ASTM-E83 [11]. Applied stress was determined from the measured applied load divided by the initial sample cross-section. Stress-strain curves were used to determine elastic modulus (E), 0.2% offset yield stress (YS), ultimate tensile strength (UTS), and percent reduction of area at fracture . Due to the large variation in YS and E, the elastic modulus could not be determined over fixed strain range. Instead each curve was plotted and the elastic modulus was determined through the initial linear portion of the curve. Once the modulus was calculated a parallel line with a 0.2% strain offset was calculated. The value of 0.2% offset yield stress was the intersection of this parallel line and the stress strain curve. Ultimate tensile strength was recorded as simply the maximum stress recorded at any one point along the stress versus strain curve. Percent reduction of area at fracture was calculated by measuring the cross sectional area at the fracture location and comparing it to the cross sectional are pre-test.

2.2.3. Heating Methods

The post-fire behavior of aluminum alloys was evaluated in this research by subjecting samples to different heating regiments, cooling them, and then measuring their mechanical properties. Two different heating methods were utilized in this research to evaluate the effects of temperature: soak time at a temperature and transient heating. This was done through isothermal heating and constant heat flux exposures, isothermal heating was performed by heating to

specific temperatures and allowing specimens to soak isothermally for different periods of time. The transient heating was performed by exposing the sample to a constant incident heat flux using a radiant heat source from a cone calorimeter. All samples were water quench cooled directly following their exposure.

Isothermal furnace heating was performed using a Blue M Electric furnace with a temperature range of 593^{o}C. Using a programmable PID controller, the furnace was maintained within +/- 0.5^{o}C. In this method, the furnace was heated to a desired temperature. Samples 19 mm in diameter were then placed into the heated furnace and heated for specified times. A sacrificial sample was placed in the furnace each time with a thermocouple attached. This sample was used to signal when the test samples had normalized to the furnace temperature. Time measurements began after the specimens had reached the desired temperature level. The heating rates imparted in the isothermal furnace averaged 21^{o}C/min with a deviation of 5^{o}C/min. "Zero time" represents that the samples were removed as soon as they reached the specified temperature. After the desired exposure the test samples were removed and immediately water quenched. Hardness measurements were made immediately following the exposure. Exposure temperatures ranged from 150 – 500^{o}C while soak times in the study included 0 – 240 minutes.

Transient heating of samples at different rates was performed using a constant heat flux exposure from an ASTM E-1354 cone calorimeter. This device was used for heating because it is regarded as a representative heating due to an exposure fire. Heat fluxes selected to represent different fire conditions were 10 kW/m^2, 20 kW/m^2, and 40 kW/m^2. Samples 19 mm in diameter were painted flat black then inset into a 25.4 mm thick piece of insulating ceramic fiber board. The transient heating of the sample was measured using a thermocouple inserted into a 2 mm hole drilled into the side of the sample as well as between the insulation board and the unexposed

side of the sample. The temperatures at the midpoint and the bottom surface were only different by 10^{o}C, but to ensure thorough and complete heating through the sample the bottom surface temperature was used. When the bottom unexposed surface temperature reached a desired temperature, the samples were removed from the constant heat flux and immediately water quenched. Hardness measurements were then performed on the bottom unexposed surface.

2.2.4. Materials

Four different aluminum alloys were tested in this study to include the effect of different types of hardening treatments and manufacturing methods in the experimental study. This research included 6082-T651 heat treated aluminum alloys as well as 5083-H116 strain hardened alloys. Tests were performed on both 6082-T651 rolled plate, 6082-T6 extruded sample, and two different sources of 5083-H116 rolled plate referred to as 5083-H116 A and 5083-H116 B.

Detailed study on the effects of heating on hardness of samples was performed using 19mm diameter samples core drilled from plates. To reduce any effect of machining, water flowed over the samples during the drilling procedure.

Tensile testing samples were taken from the parent material such that the longitudinal axis of the specimen would be parallel to the rolling or extrusion direction. Sample dimensions are summarized in Table 1. To ensure that the specimens had a parallel gage length and square ends, slightly oversized rectangular blocks of material were machined down to the proper tensile testing specimen profile using a vertical mill.

Table 1 Tensile Test Specimen Gage Dimensions

Material	Gage Width (mm)	Gage Thickness (mm)
5083-H116 A	12.7	4.85
5083-H116 B	12.7	6.10
6082-T651	12.7	8.08
6082-T6 Extrusion	12.7	3.91

2.2.5. Testing Overview

Tensile testing was done on samples of all four materials. These samples were first isothermally heated, with a zero soak time, then tested. Testing started with hardness values being measured with the bench top hardness tester. After hardness values were recorded, the samples were loaded in tension until failure.

The isothermal testing contained both samples solely for Vickers hardness and flat tensile test samples. The Vickers hardness samples for all four specimens were 19 mm diameter core drilled samples. After machining the samples were heated, quenched, cleaned, and then had Vickers hardness measurements performed. For tensile test samples isothermal heating was the only method employed for all four specimens. The samples were machined, heated, quenched, cleaned, had their hardness measured, and then tensile tested until failure.

Constant heat flux testing was performed only on 19 mm core drill samples as a means of validating the use of isothermal heating for fire testing. Samples were core drilled, painted flat black, exposed to the heat flux, quenched, cleaned, and then hardness testing was performed.

2.3. Results

Data is provided on the static tensile properties and hardness of meterials following various elevated temperature exposures. Tensile testing provided measurements of modulus of elasticity, yield stress, ultimate tensile strength, and percent elongation. Detailed evaluation of exposure duration on sample property was evaluated through hardness testing.

2.3.1. Post Fire Tensile Tests

Flat tensile test specimens were immersed in an elevated temperature environment for increments of time after reaching equilibrium. Each specimen was isothermally heated with zero soak time, water quenched then tensile tested.

2.3.1.1. Stress-Strain Curves

Stress – strain curves for the different types of aluminum alloys exposed to different levels of heating are provided in Figures 1 -4. The 5083-H116 strain hardened materials stress-strain curves are given in Figures 1 and 2. These materials were measured to have pronounced oscillations in the plastic region of the curve. This has been attributed to slippage along large grain boundary slipping, and has been shown in results from other researchers at low temperatures [5,16]. With an increase in exposed temperature, the onset of the oscillations in the 5083-H116 material is seen in Figures 1 and 2 to decrease from 5% strain at room temperature to 1% strain for a sample previously exposed to 500^{o}C. The stress-strain curves for heat treated 6082-T6 alloys are seen in Figures 3 and 4 to only display this behavior following an exposure at 500^{o}C.

2.3.1.2. Modulus of Elasticity

Figure 5 contains the results for modulus of elasticity results for all the specimens. The American Society of Metals states that the Young's modulus for 5083 should be 70.3 GPa [17]

and Eurocode 9 lists it at 70.0 GPa for all alloys [2]. The results from our testing did not yield values near this. Sources for this difference, up to 30%, were from the use of a high strain extensometer that had less accuracy than other instrumentation possibilities. Additional testing with strain gages yielded modulus values in the appropriate range, and verified inaccuracy in the extensometer used. While the numerical values calculated for modulus of elasticity were affected by this inaccuracy, the 0.2% yield stress values varied only slightly with the modulus of elasticity value. Figure 5 shows that while both 5083-H116 A and 5083-H116 B never possess less than 75% of their room temperature modulus, the trends are different. 5083-H116 A maintains a nearly constant modulus value until the exposure temperature exceeds 300^{o}C, where it begins to decline towards its final value of 53.4 GPa. The modulus values for 5083-H116 B remained unchanged to 150^{o}C but declines at 300^{o}C. At temperatures 300^{o}C and greater the modulus remains at approximately 52 GPa.

The 6082 alloys exhibited a different trend than the 5083. The 6082-T651 samples had modulus values that remained constant up to 250^{o}C the decreased to a minimum value of 33 GPa at 400^{o}C. After heating to 500^{o}C the modulus recovered to a value of 62 GPa. The same general trend in the modulus was measured for the 6082-T6 extrusion except some modulus increase was measured after low temperature heating to 150^{o}C.

2.3.1.3. Yield Stress

The calculated 0.2% offset yield stress values for zero soak time samples are displayed in Figure 6. All four specimens demonstrate a trend for decreasing yield stress as pre-test exposure temperature increases from room temperature to 500^{o}C.

Both 5083-H116 plates exhibit a nearly linear decline from room temperature to the pre-test exposure temperature of 500^{o}C. The yield stress for 5083-H116 B is higher compared with

yield stress for 5083-H116 A. Despite this difference, both retain 50% of their unheated yield stress values.

The 6082-T651 plate and 6082-T6 extrusion have unheated values that were approximately 30% higher than the 5083-H116. Yield stress for 6082 remains at unheated levels for the pre-test exposure temperature up to 250°C. From 250°C to 400°C, both 6082 specimens have at least 60% loss in residual yield stress. The 6082 alloys exhibit the lowest residual yield stress values at 400°C with an increase in yield stress when the pre-test exposure temperature was increased to 500°C. 6082 extrusion gains 20% in yield stress between 400°C and 500°C while, 6082-T651 plate shows only a 7% gain. At 500°C all four specimens have values between 109 MPa and 132 MPa, with the non-heat treatable alloys providing the constraints for this range.

2.3.1.4. Ultimate Tensile Strength

Displayed in Figure 7 are the ultimate tensile stress values of each sample at different pre-test exposure temperatures. 5083-H116 A and B have a near linear decline in ultimate tensile strength as exposure temperature increases. By 500°C, 5083-H116 A and B had decreased 15% and 12%. 5083-H116 B has an ultimate strength that is about 10% higher than 5083-H116 A at all temperatures.

The 6082 alloys exhibited constant ultimate tensile strength up to 150°C, then a decrease in values from 250°C – 400°C. Above 400°C, both 6082 alloys recover to an ultimate tensile strength of approximately 240MPa. The ultimate tensile strength values for 6082-T651 plate and 6082-T6 extrusion are within 5% except in the 250 – 400°C exposure temperature range. In this temperature range, 6082-T651 plate ultimate strength is 17% less than strength levels of the 6082-T6 extrusion. The recuperation of ultimate tensile strength from 400-500°C is greater for

6082-T6 extrusion with a 32% increase in residual ultimate tensile stress compared with a 18% for the 6082-T651 plate.

All specimens except 5083-H116 B have similar ultimate tensile strength values at the temperatures up to 250°C. Above a pre-test exposure temperature of 250°C, 6082-T6 specimens have a lower ultimate tensile strength compared with the 5083 alloys. At 500°C, the specimens are banded with 5083-H116 B being the highest at 300 MPa, 5083-H116 A being 280 MPa, and both 6082-T6 alloys being the lowest at approximately 240 MPa.

2.3.1.5. Reduction of Area at Fracture

During tensile testing all of the aluminum samples experience high amounts of local necking. Because the necking was high and concentrated to only a small portion of the gage length, percent reduction of area was used instead of percent elongation as a measure of the amount of deformation in samples. Post-testing samples were measured with calipers, +/- 0.0254 mm, at the fracture location to determine cross sectional area. Subtracting the post-test area from the pre-test area, known from documentation, and dividing by the pre-test area gave a percent reduction in area at the failure.

A plot of the percent reduction of area at fracture for each material at different pre-test exposure temperatures is provided in Figure 8. The 5083-H116 alloys both display the same trend. At 150°C the percent reduction of area values are low; 26% for 5083-H116 A and 20% for 5083-H116 B. As the temperature increased the percent reduction in area increased for both the 5083-H116 A and 5083-H116 B alloys in a linear fashion. At 500°C the maximum percent reduction in area occurs with 5083-H116 A having a value of 32% and 5083-H116 B having a value of 25%. The final value for 5083-H116 B was 5% higher than the room temperature value but was identical to the 5083-H116 A 150°C value.

6082-T651 starts out with much higher percent reduction of area values, 34%, than seen in the 5083-H116 alloys. As temperatures increase so does the percent reduction of area for 6082-T651. The maximum percent reduction of area, 42%, occurs at 350°C. At 500°C the reduction of area is only 5% higher than the room temperature value. 6082-T6 Extrusion displays a much different trend as it starts at only 25% reduction of area. The percent reduction of area decreases until temperatures reach 300°C, with a minimum value of 21% at 250°C. There is a 22% increase at 300°C with the percent reduction of area jumping to 43%. Between 300°C and 500°C the percent reduction of area decreases linearly with temperature. At 500°C the percent reduction of area is 9% higher than the room temperature value.

2.3.2. Hardness

Vickers hardness measurements were performed on samples that were heated in various ways to quantify the change in material properties. Measuring the Vickers hardness (HV_5) before and after exposure to temperature created a discernable trend between residual hardness measurements and exposure temperature. The use of the isothermal furnace and constant heat flux heating methods was used to quantify the sensitivity of heating rate and exposure time to residual hardness.

2.3.2.1. Isothermal

All four materials were tested in isothermal heating conditions at various temperatures and durations to quantify the effect of heating on Vickers hardness. Initial heating rate to furnace temperature was on average 21°C/min. Figure 9 contains the results for 5083-H116 A and 6082-T651 plate at different exposure temperatures and durations. In Figure 9a, 5083-H116 A maintains a hardness of approximately 95 HV_5 until 250-300°C and then decreases between 250-350°C to a second plateau of 78 HV_5. Looking at the variation between duration of exposure, the

data indicates that 5083-H116 has nearly no dependency on exposure duration except at 300°C where the change in properties is occurring.

The 6082-T651 alloy data seen in Figure 9 b have a higher room temperature hardness value compared to 5083-H116. However, due to the temperature hardening of the 6082-T6, it begins losing strength at 200°C and decreases by a larger percentage compared to the strain hardened 5083-H116. In addition, 6082-T6 exhibits a different change in hardness with increase in temperature. Hardness remains constant at 111 HV_5 up 150°C and then declines to 34-44% of room temperature hardness. When the exposure temperature is increased to 500°C, the hardness increases resulting in a 70% reduction over values at room temperature.

The time dependence for the 6082-T6 alloy is also more evident, especially for tests within the 200-400°C temperature range. The difference between the zero time results and the results for samples with long soak times were 12% at 250°C, 21% at 300°C, 14% at 350°C, and 8% at 400°C and 500°C. This is most evident at 300°C where the hardness value changes by 17 HV_5 between the zero and fifteen minute exposure duration and continues to decrease as the exposure duration increases. Subsequent times show further decreases in residual hardness but by 13 HV_5 total for all series after the initial fifteen minutes.

Figure 10 contains a plot of Vickers hardness for all specimens at different exposure temperatures with a zero time heating duration. The hardness values for 6082 alloys fall within 4 % for all exposure temperatures, except at 400°C where the difference is 13%. The two 5083-H116 alloys were measured to have a similar response with increase in exposure temperature but the 5083-H116 A is within standard deviation to the 5083-H116 B. Note that from 300-400°C, the 6082-T6 alloys have a residual hardness less than that of 5083-H116 alloy. However, all materials were measured to have the same hardness of 75 HV_5 at 500°C.

2.3.2.2. Constant Heat Flux

Fire exposures are typically represented by a constant heat flux exposure which results in a transient temperature rise of the material. Constant heat flux tests were performed using the radiant heat source from the cone calorimeter with incident heat fluxes of 10 kW/m^2, 20 kW/m^2, and 40 kW/m^2. With isothermal furnace heating, an average heating rate of 21^{o}C/min could be achieved averages of 29^{o}C/min, 61^{o}C/min, and 222^{o}C/min were achieved with constant heat flux exposure of 10, 20, and 40 kW/m^2; respectively.

Figure 11 contains results of measured hardness values following the constant heat flux exposure for the 5083-H116 A and 6082-T651. Also shown in these plots are the hardness values measured for specimens with isothermal heating and zero time exposure duration. The zero time isothermal series was selected for comparison because the heat flux test samples were removed from the cone calorimeter after reaching the desired temperature similar to what was done in the isothermal zero time samples. For 5083-H116 A samples, the transient heating results were within 7% of the isothermal test results except at 300^{o}C where there was a 17% difference. In addition to following the same trend, the 5083-H116 A exhibits nearly the same values whether exposed to heat flux or isothermal heating. This may be expected based on the lack of time dependence observed during the isothermal testing as shown in Figure 9a and Figure 9b. The 6082-T651 plate follows a similar trend when exposed to heat flux as to when isothermally heated. Both heating methods resulted in a decrease in hardness of 40% for 6082-T651 as the exposure temperature was increased from 150^{o}C - 350^{o}C; however, magnitudes of these changes were not consistent. These differences are attributed to the increased time dependence for the 6082-T6 alloys between 200^{o}C and 500^{o}C.

2.4. Discussion

2.4.1. Effect of Heating on Mechanical Properties

Exposure to elevated temperatures above 150°C for 6082 alloys and 250°C for 5083-H116 for any amount of time results in a change in mechanical properties for both the 5083 and 6082 aluminum alloys. Yield stress and ultimate tensile strength were affected significantly by the increase in exposure temperature. For both 5083-H116 plates, a minimum value of residual yield stress occurs at 500°C. The 5083-O annealed state has values of $YS \geq 125$ MPa and $UTS \geq 275$ MPa[18], which is similar to values at 500°C. The annealing temperature for 5083 is 415°C[18]; which explains why the 500°C values of the 5083-H116 plates, are comparable to the "O" annealed state values. Because the hot working temperature begins about 100°C before the annealing temperature, material properties start deteriorating before the material anneals [19].

The 6082 alloys were measured to have the largest proportional loss in yield stress with the minimum values are achieved at 400°C. From 150°C to 400°C, the 6082 alloys exhibit a significant and sustained decline in yield and ultimate tensile stress values. The heat treatment aging temperature for 6082 is 175°C [20]. Since both 6082 alloys have a T6 treatment, no additional strength was gained from aging the material any longer. At 415°C 6082 becomes fully annealed. This explains why the minimum values for yield stress and ultimate tensile stress occur at the 400°C test point. At 400°C, properties for the 6082-T651 plate are $YS = 101$ MPa and $UTS = 180$ MPa. This is similar to the 6082-O values from EN-755-2; $YS \geq 60$ MPa and $UTS \leq 130$ MPa [20]. It becomes apparent that the large losses in residual yield and ultimate stress are the effect of annealing the material. The regaining of property values at the 500°C test point are due to the material approaching the solution heat treatment temperature, 565°C, where all the

precipitates will reenter the aluminum solution allowing the material to be heat treated again [19].

2.4.2. Relationship between Mechanical Properties and Hardness

A linear relationship between Vickers hardness and yield stress has been described by Tabor [7],

$$HV = c * Y \quad (4)$$

where the linear slope coefficient, *c* has been quoted to range between 2.9 and 3.2 [7]. This research explored applying this linear relationship to post fire aluminum specimens as a means to quickly determine material properties.

The use of aluminum alloys presented several deviations from the linear equation stated above. The first is that Tabor formed this relationship assuming pure elastic-plastic response to strain. Secondly the relationship was formulated with a non-strain hardening material. Figure 12 shows the relationship between Vickers hardness and 0.2% offset yield stress. Note that yield stress is in units of MPa, which makes constant *c* have units of acceleration (m/s^2). Performing a linear regression through the 5083-H116 plate data, Figure 12, without an intercept leads to a negative r^2 value. For the 6082 alloys setting the intercept to zero and calculating a linear regression gives decent accordance, $r^2 = 0.69$ and a slope in the region that was described by Tabor. Statistics for the linear regression were calculated for all samples combined yielding a slope of 0.258, an $r^2 = 0.87$, and a positive intercept of 37.5. The correlation of Vickers hardness to 0.2% offset yield stress of 5083-H116 and 6082-T651 was utilized by implementing a non-negative intercept. To keep with the convention of an intercept of zero, other correlations to Vickers hardness were evaluated.

These inconsistencies with the model stated in Equation 3 and the data arise from the nature of aluminum alloys. Aluminum consistently does not exhibit elastic-plastic behavior and most alloys will strain harden to some degree. To correct for these issues it has been suggested to calculate Equation 3 not from the yield stress, but from some stress at a constant offset strain value. Tabor suggests 8% strain, while Tekkaya empirically arrived at 11.2% strain [7,21].

Figure 13 contains a plot of the Vickers hardness versus stress at 8% strain for all four specimens used in this research. The agreement of this graph with Equation 3, is much better than with the 0.2% proof stress. The slope for the linear regression in Figure 13 comes out to equal 3.13, which is between the values of *c* that Tabor published and the goodness of fit has also increased to $r^2 = 0.86$ for all specimens in the study.

The 8% strain offset stress is not a useful engineering quantity and is not a commonly recorded property. The ultimate tensile strength values occur very close to 8% strain. Therefore the relationship between ultimate tensile strength and Vickers hardness was evaluated. A plot of ultimate tensile strength and Vickers hardness for all materials is given in Figure 14. The value of *c* by use of linear regression returns a value of 2.94 for the slope and an $r^2 = 0.79$. The value of *c* is close to that recommended by Tabor and similar to the 8% strain result.

2.5. Summary of Findings

This research focused on investigating the use of non-destructive hardness testing as a means to predict residual mechanical properties of fire exposed aluminum alloys. To achieve this characterization, physical material properties; modulus of elasticity, yield stress, ultimate tensile strength, and percent elongation were measured after samples were exposed to fire conditions. Fire conditions were simulated by affecting the heating rate, exposure temperature, and exposure

time through the use of two different heating methods. Finally the correlation between residual hardness and yield stress values for fire exposed aluminum alloys was conducted.

The response of residual mechanical properties, measured in terms modulus of elasticity, yield stress, ultimate tensile stress, and percent elongation at fracture, was characterized in response to elevated temperature and time at elevated temperature. 5083-H116 and the 6082-T6 alloys reacted to each factor uniquely, yet some similarities exist. First, exposure temperature is much more detrimental to residual properties than is the time for which the sample was maintained at that temperature. Significant impacts on time were limited to a few temperatures near the annealing temperature for the 6082 alloys, but after fifteen minutes of exposure further exposure had near zero impact on to residual values. Second, none of the specimens in this research displayed properties less than their annealed state. While significant differences between the annealed state and the baseline state can exist particularly for the 6082 T6, the material always retains a certain level of strength. The final similarity is that within the alloy, the specimens behaved near identical. Both the 5083-H116 A and 5083-H116 B plates demonstrated like values for residual measurements; the same goes for the 6082-T651 plate and 6082-T6 extrusion. Even when values were not exactly the same, the materials demonstrated similar trends though the absolute magnitudes may have been different.

Yield stress does exhibit a dependence on Vickers hardness, but this trend incorporates a positive intercept on the y-axis, Vickers hardness, denoting that a material with a 0 MPa yield stress would still possess a positive Vickers hardness value. This is physically not possible. The positive intercept also seems to be material dependent, with the 5083-H116 posting a different intercept than the 6082 alloys. It was possible to accurately predict the stress at 8% strain. Unfortunately this is not a helpful quantity, for several of the tests in this research 8% strain

occurs after the ultimate tensile stress has been surpassed, meaning that the sample was failing. In addition the relation of stress at 8% strain to the desired quantity, 0.2% proof stress, is neither linear nor predictable. The relationship of ultimate tensile strength, used because the 8% offset strain tends to be very near the strain at ultimate tensile stress, provides a very good linear fit.

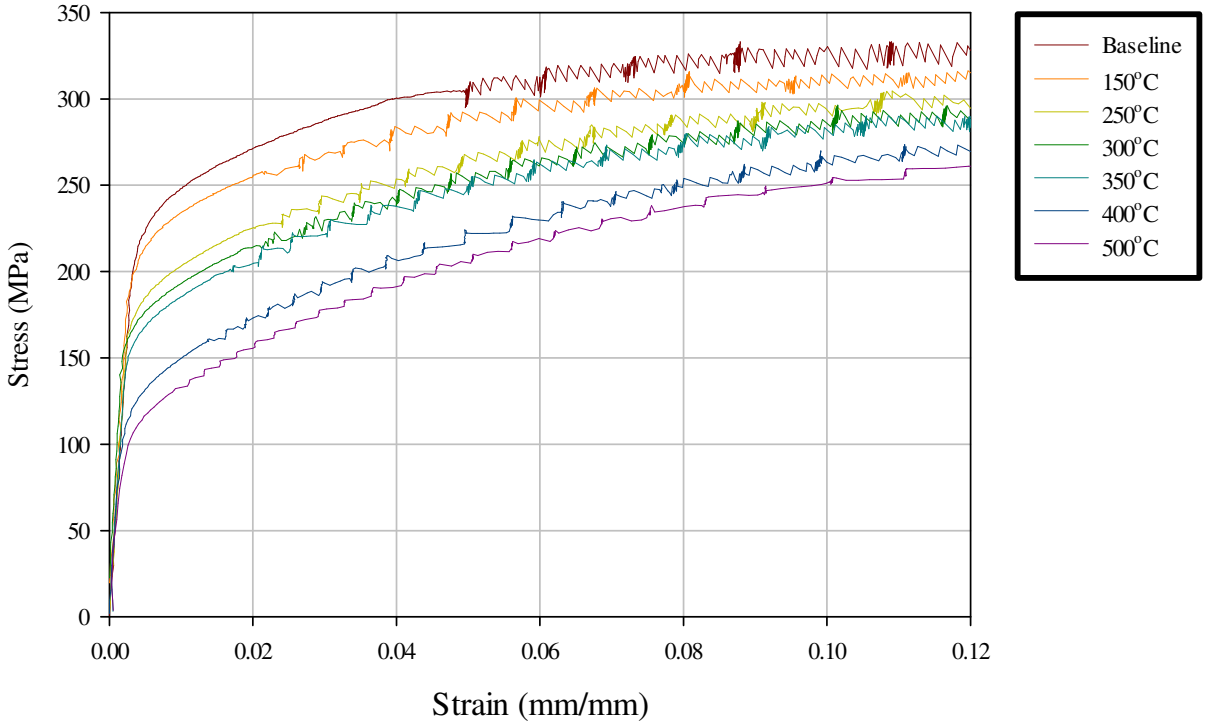

Figure 1 Tensile Testing Results for 5083-H116 A

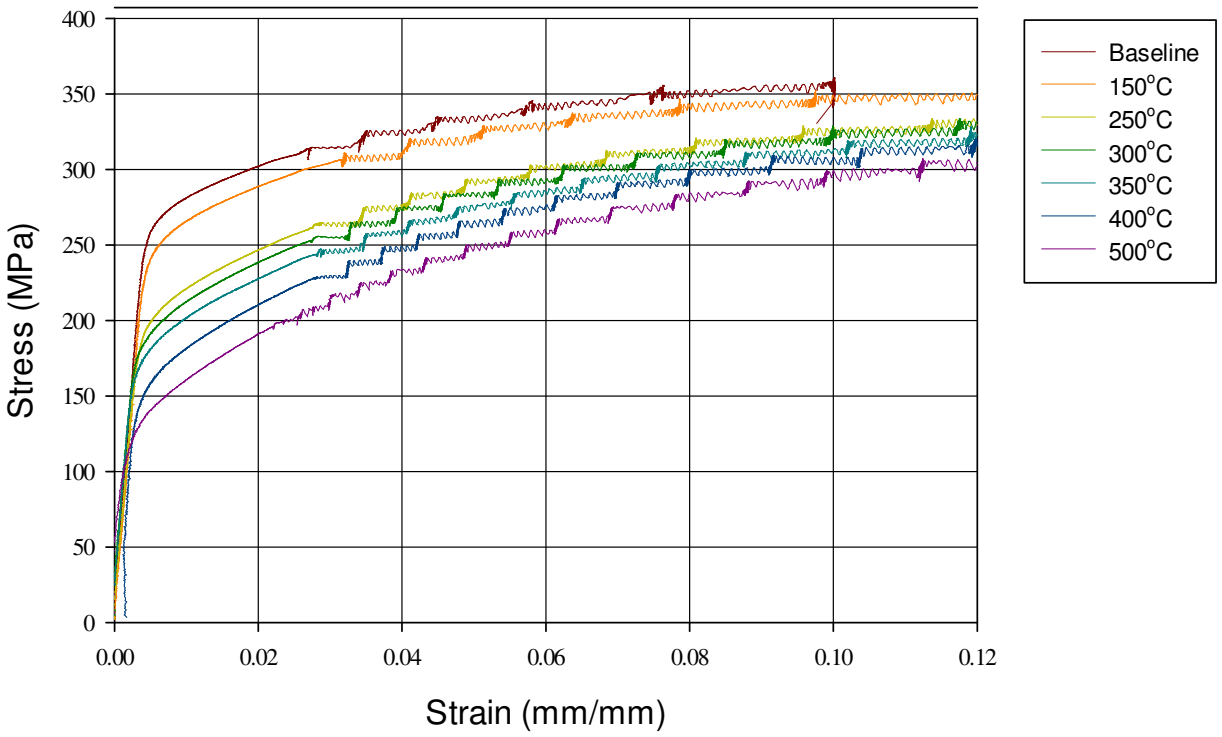

Figure 2 Tensile Test Results for 5083-H116 B

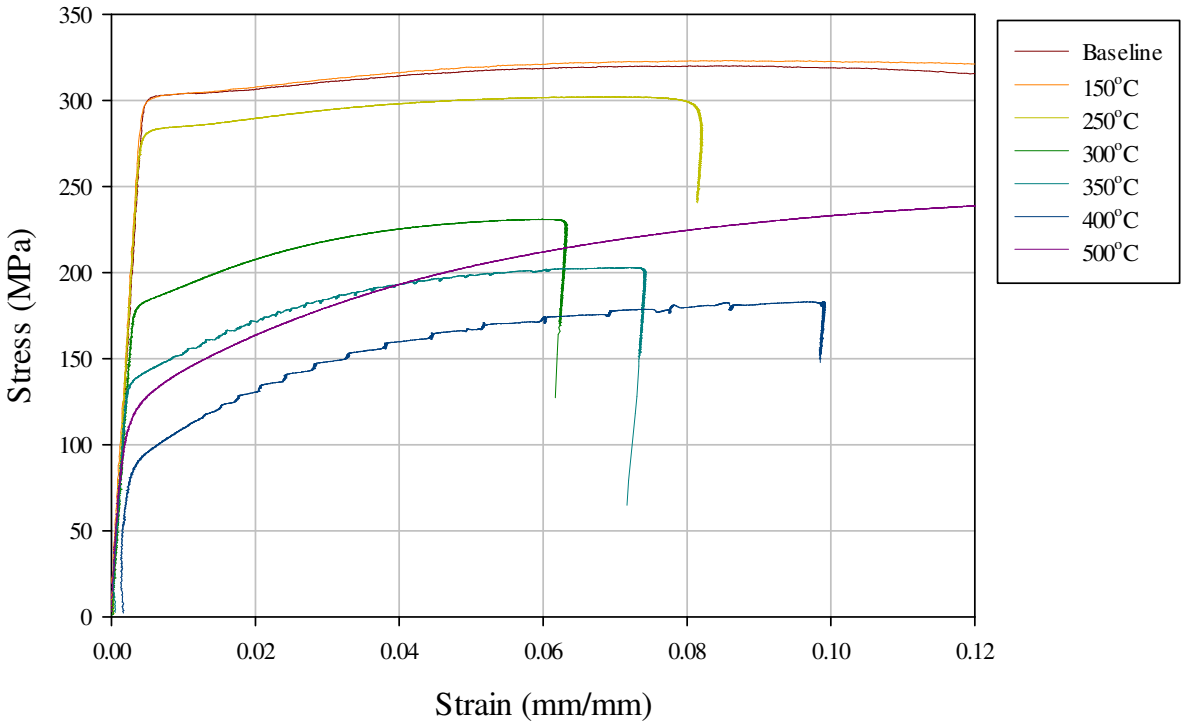

Figure 3 Tensile Testing Results for 6082-T651 Plate

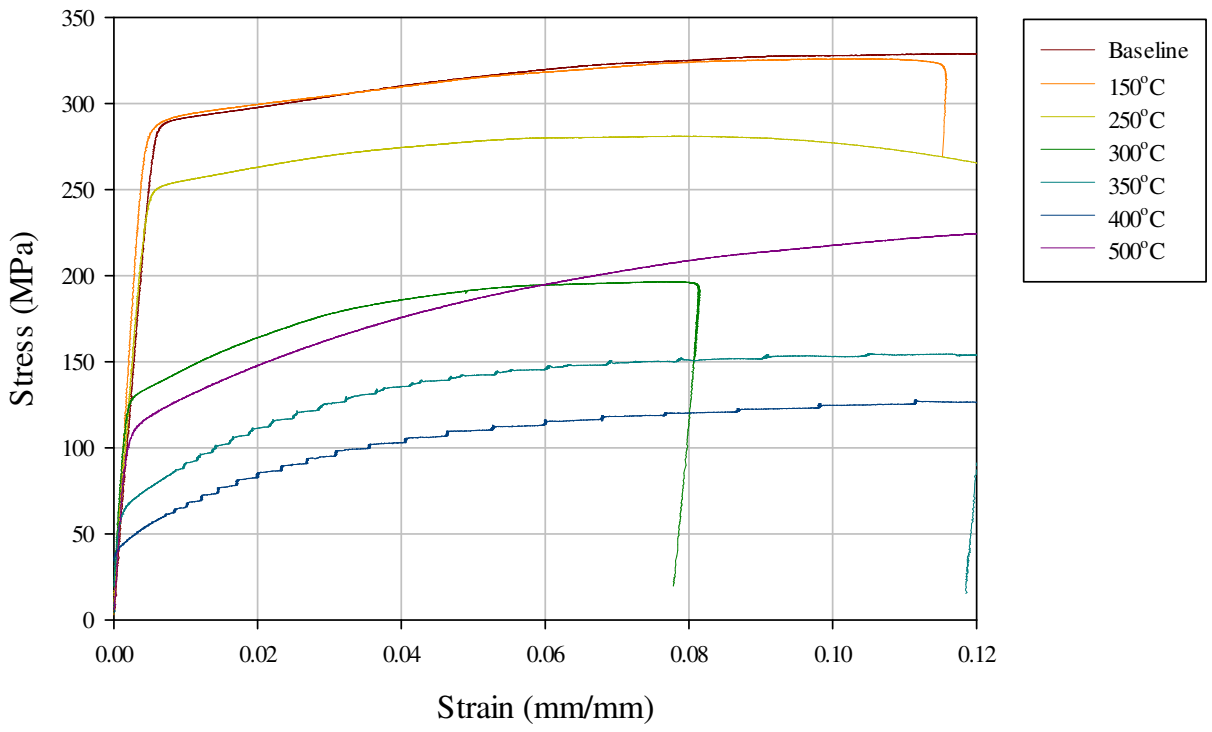

Figure 4 Tensile Test Results for 6082-T6 Extrusion

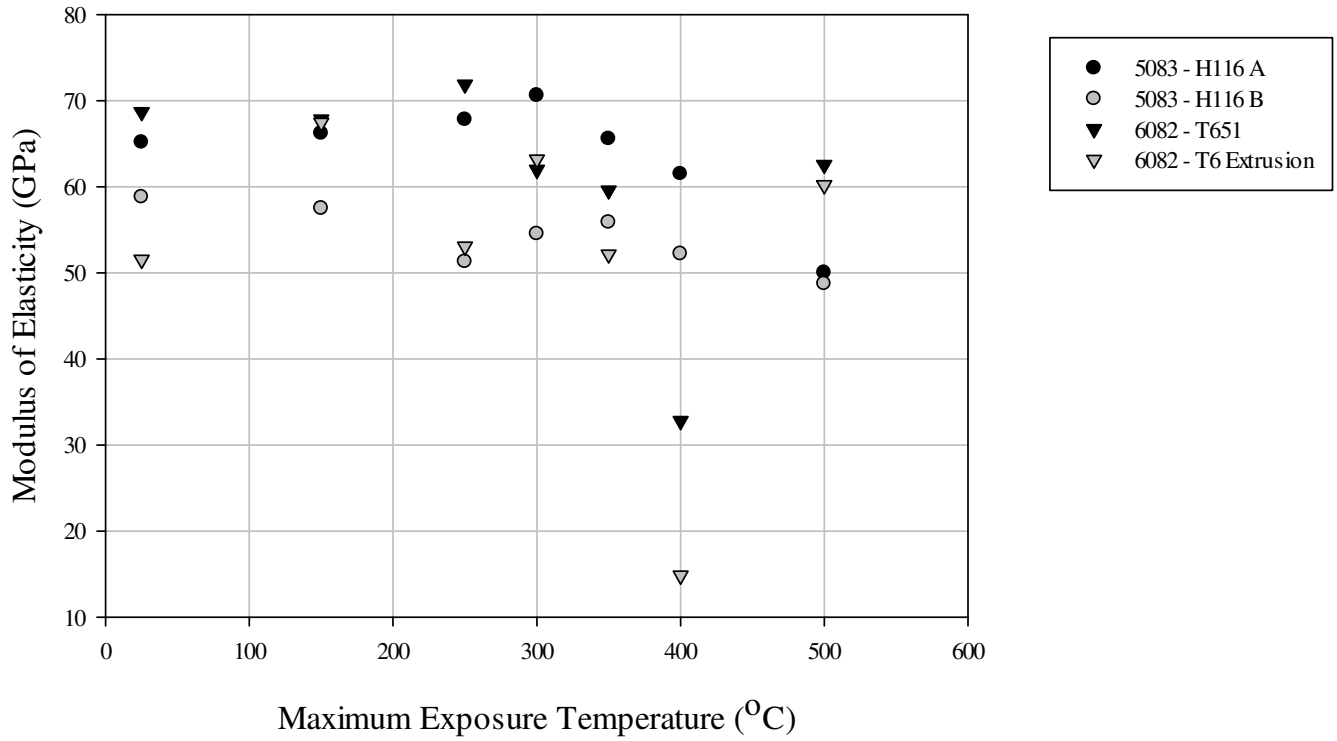

Figure 5 Modulus of Elasticity of All Test Samples

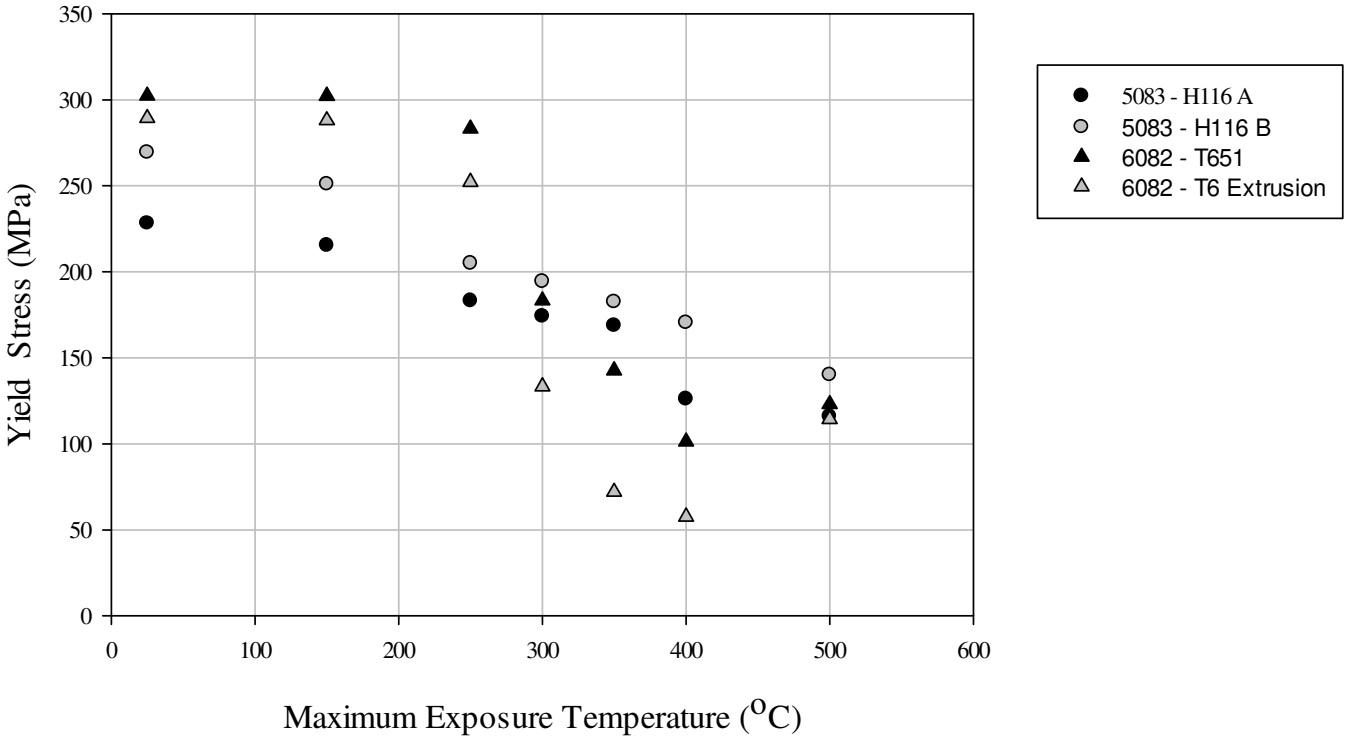

Figure 6 0.2% Yield Stress Results for All Samples

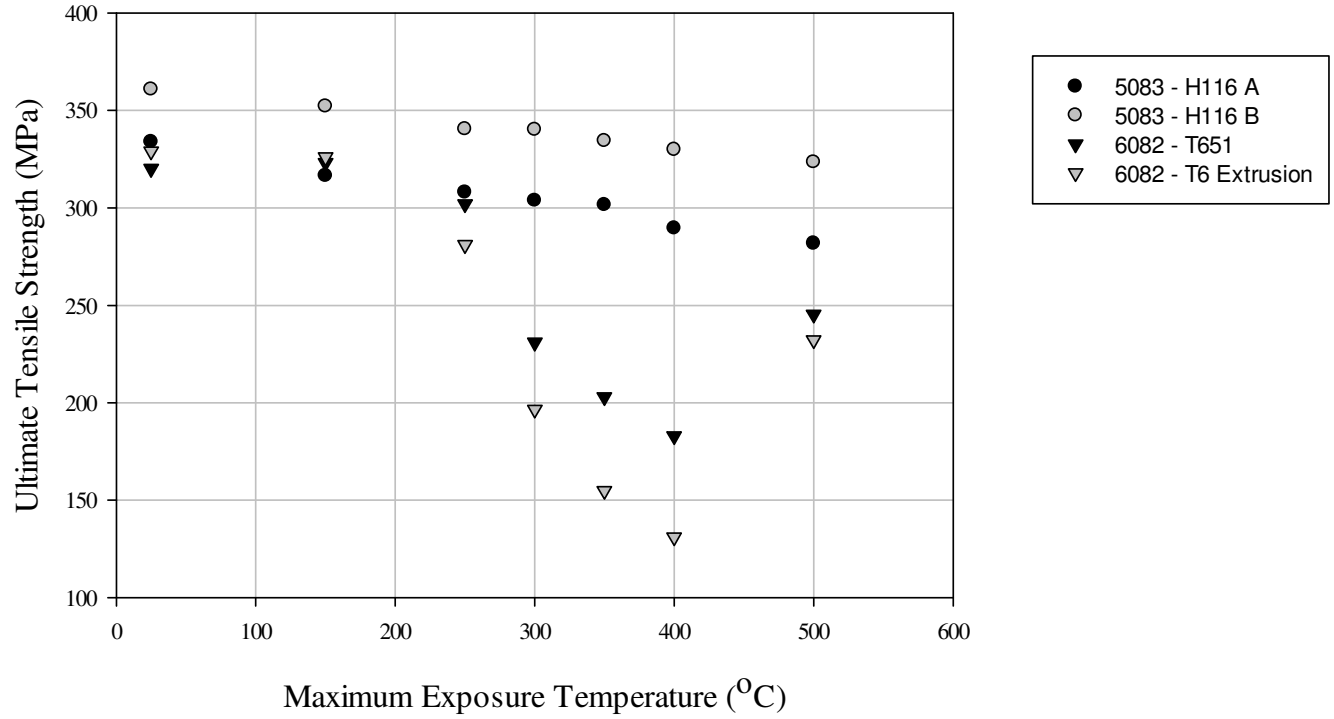

Figure 7 Ultimate Tensile Strength

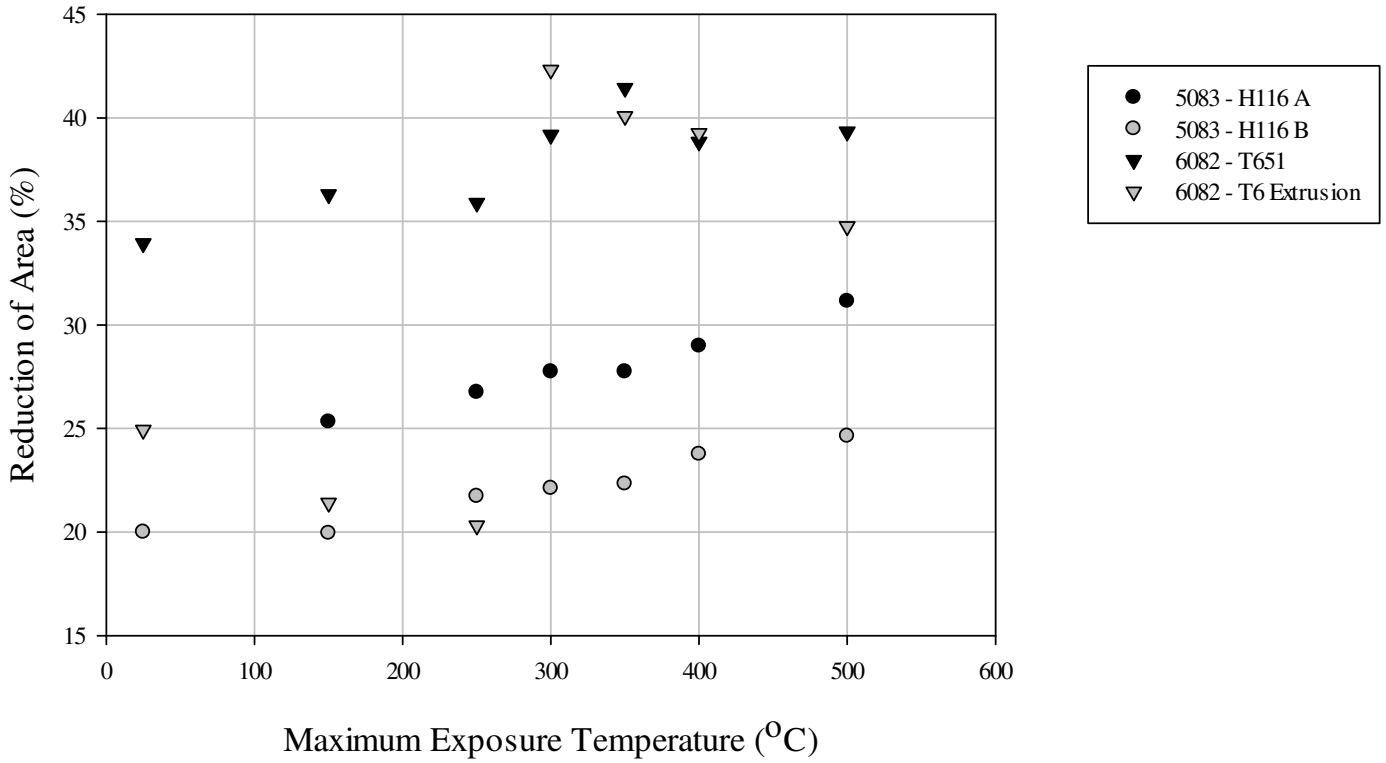

Figure 8 Reduction of Area

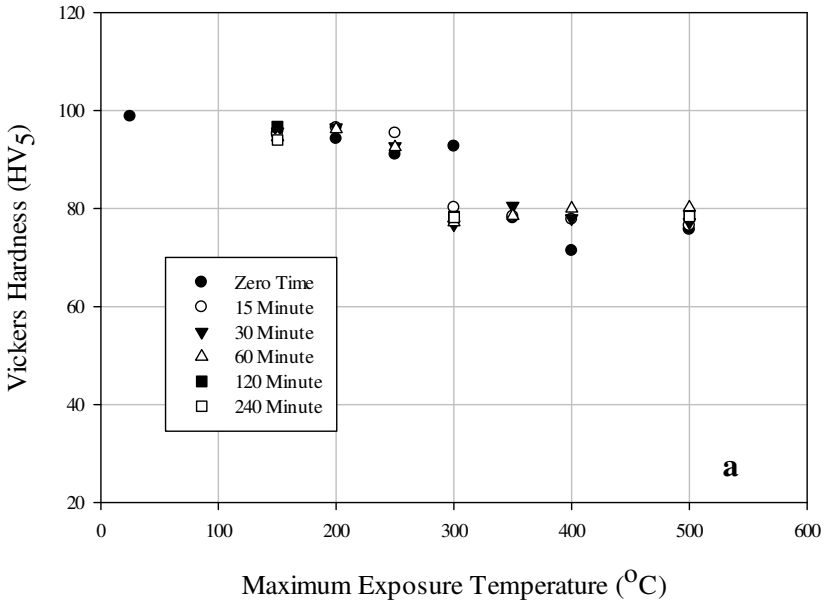

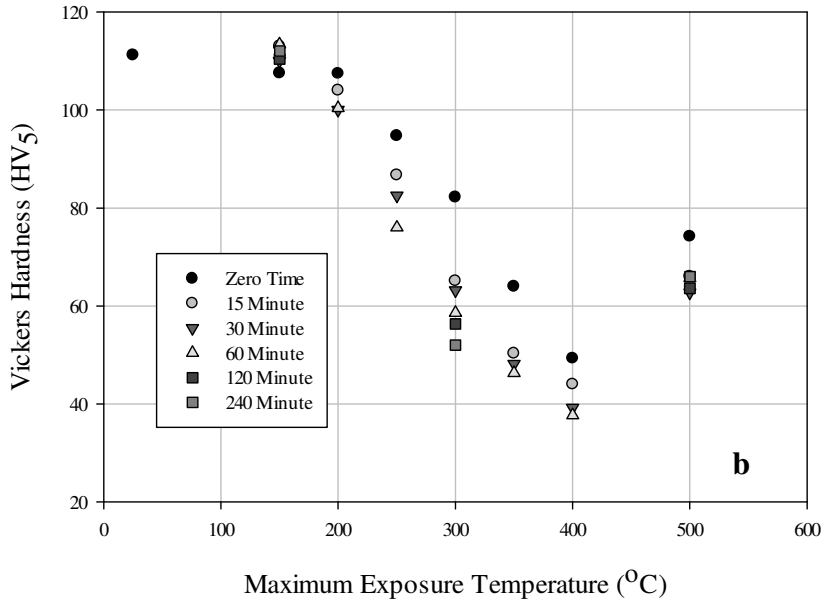

Figure 9 Isothermal Vickers Hardness for (a) 5083-H116 A and (b) 6082-T651

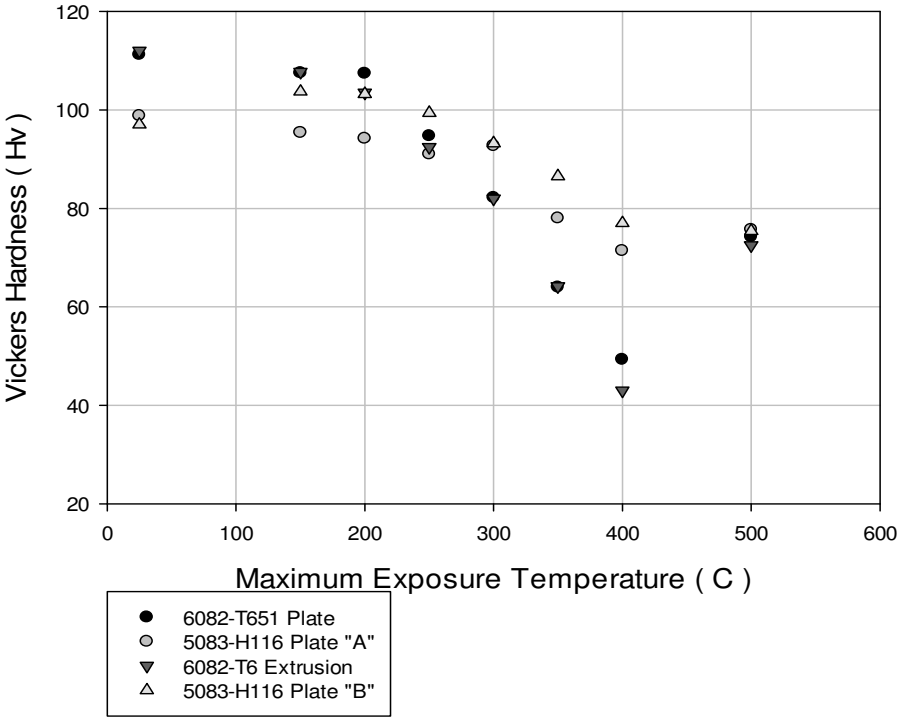

Figure 10 Comparison of Vickers Hardness for All Materials at Zero Time

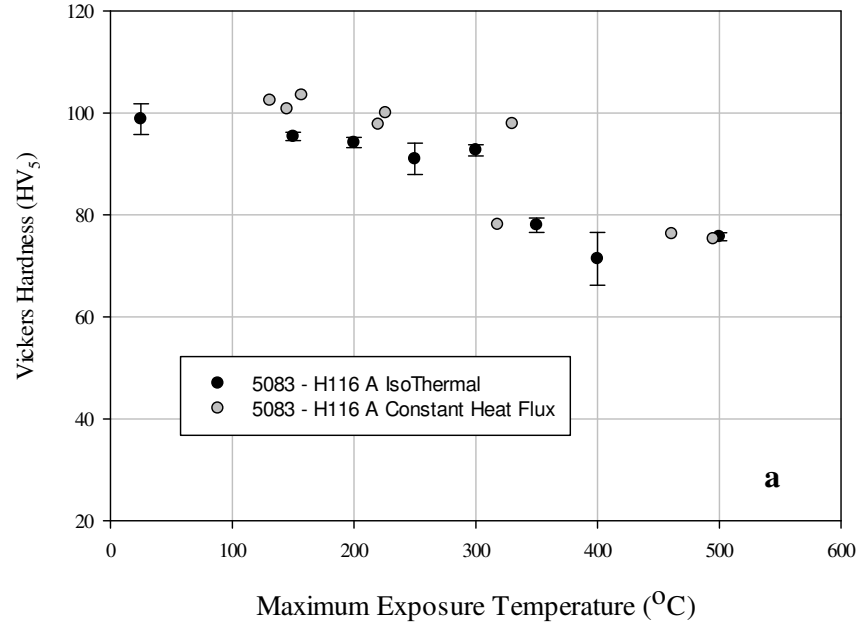

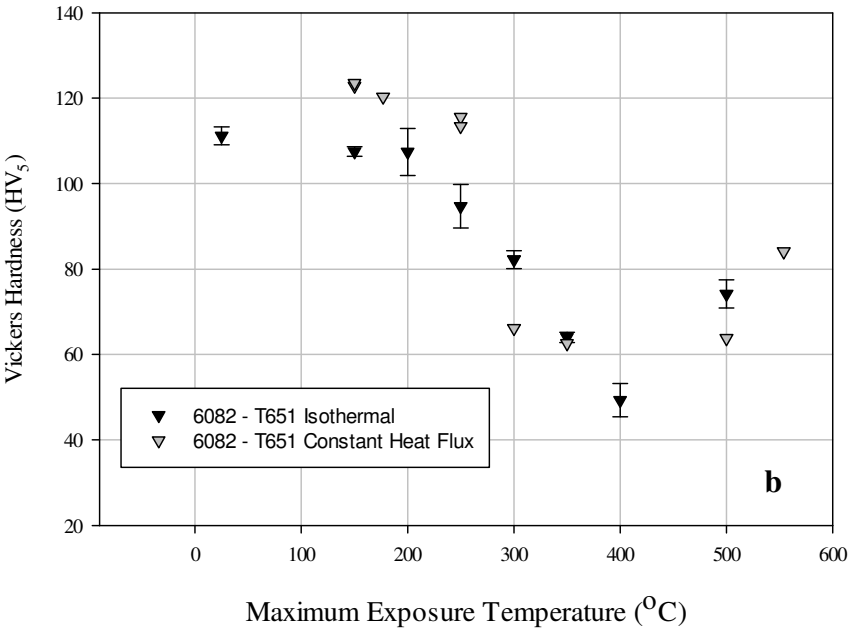

Figure 11 Constant Heat Flux Vickers Hardness for (a) 5083-H116 A and (b) 6082-T651

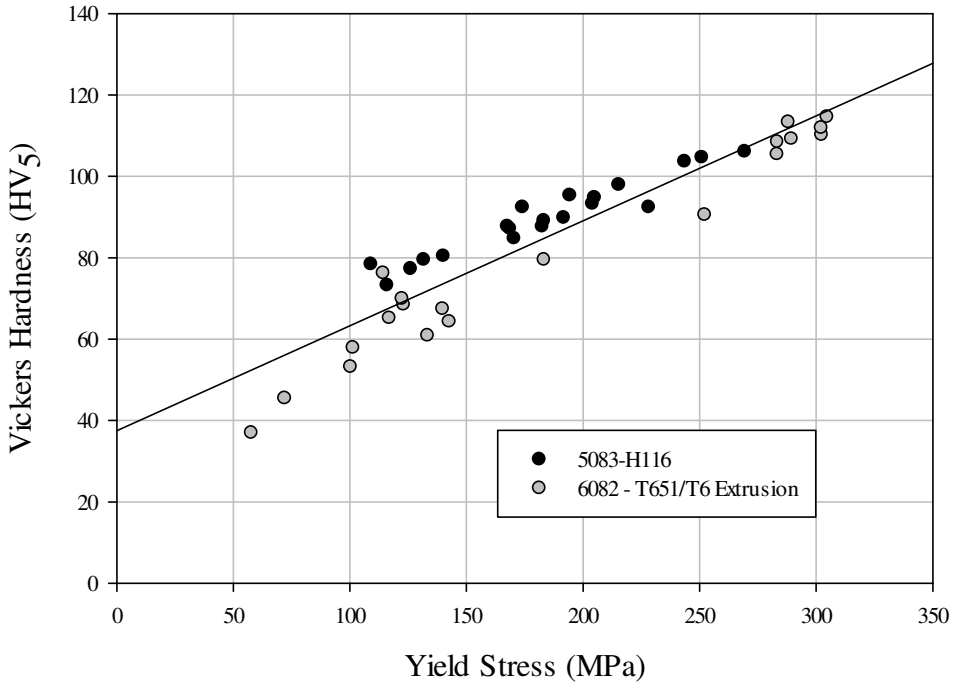

Figure 12 Relation of Vickers Hardness to Yield Stress

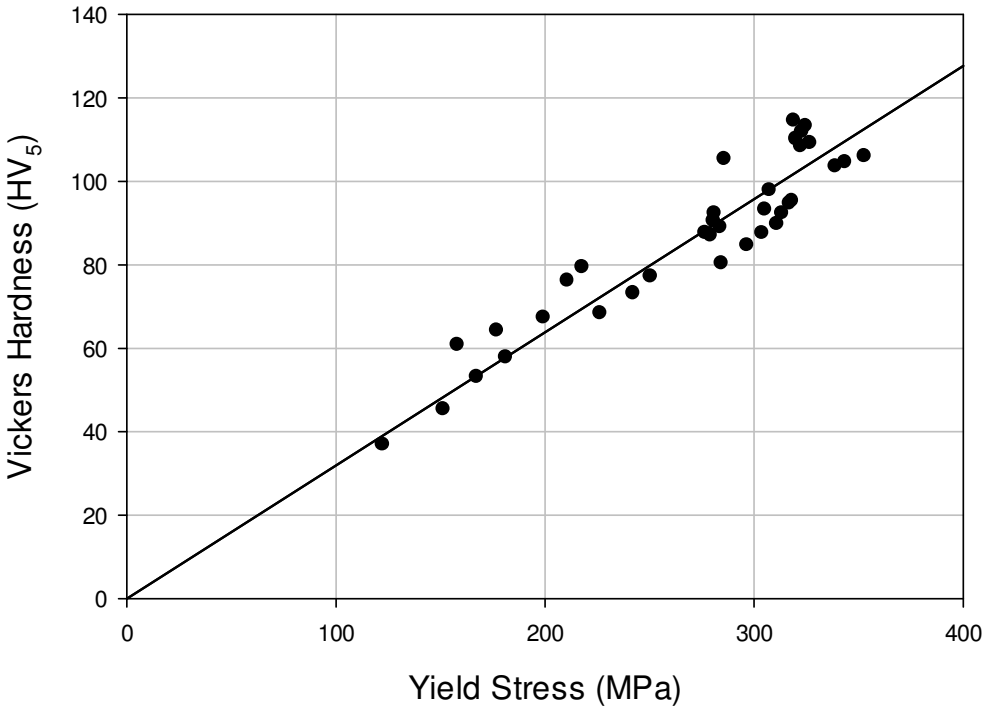

Figure 13 Vickers Hardness Versus Stress at 8% Strain

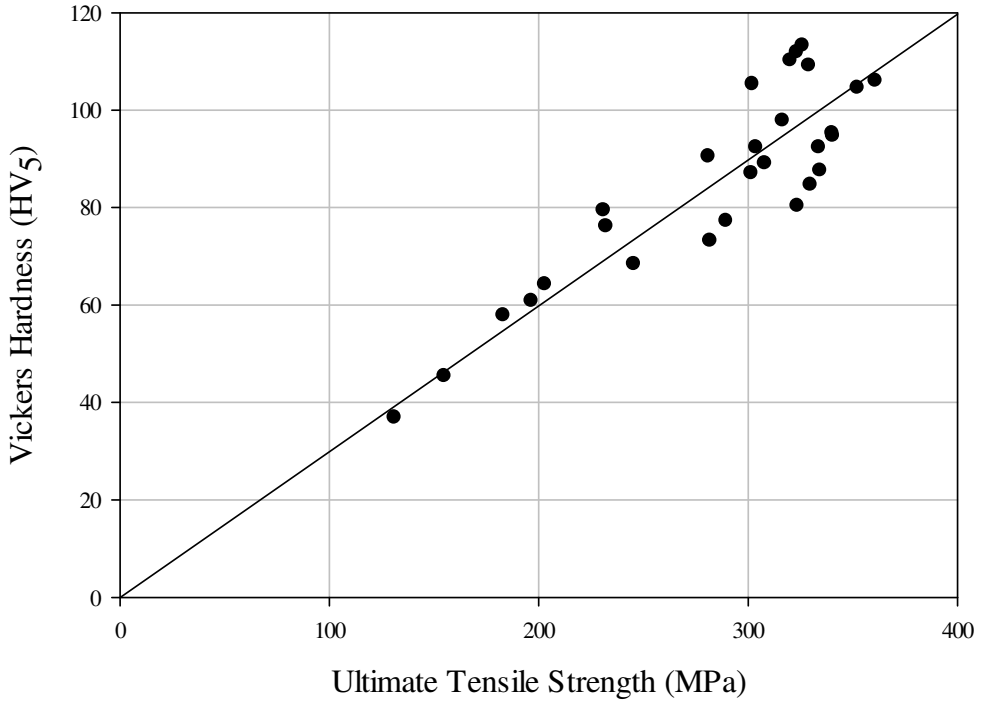

Figure 14 Vickers Hardness Versus Ultimate Tensile Strength

3. POST HEATING EFFECTS ON WELDS

3.1. Introduction

Aluminum structures offer a lightweight alternative in modern structural designs. By replacing components that are conventionally constructed of steel with aluminum components a considerable amount of weight may be saved. The low weight, combined with its high natural resistance to corrosion has seen aluminum alloys being extensively deployed in the construction of load bearing structures. Some research has been done to determine the static properties of welded aluminum alloys. The width of heat affected zones is outlined in Eurocode 9[2] and relationships of the residual stress in square columns with relation to HAZ is described by Maljaars *et al*[5]. Tensile properties of parent material, HAZ material, and the weldment itself were performed by Collette[22]. The width of heat affected zones has been mapped by using hardness measurements in a spatially discretized pattern moving from virgin material through the heat affected zone and weld as seen in Hartawan *et al*, Pereira *et al*, and Paik *et al*[23-25]. By combining the material properties of the virgin material, the heat affected zone, and the weldment with the physical hardness, this research aims to address the concerns of post fire characterization of welded aluminum alloys.

3.2. Experimental

3.2.1. Tensile Testing

Tensile tests were performed in an Instron tensile test frame, Model # 4468, equipped with a 150 kN load cell. Tests were performed using displacement control at a rate of 2.54 mm/min to provide smooth and consistent test results[12-14]. With the samples being extracted from Configurations 1 and 2, flat tensile test samples were machined according to ASTM B-

557[15]. Sample thicknesses were 4.115 mm and 6.2mm depending on which configuration they were extracted, Figure 15 or Figure 16.

Samples used in this study had overall length of 203.2mm, width of 25.4mm, gage length of 50.8mm, and gage width of 12.7mm. The sample thicknesses were slightly less than that of the thickness of the extraction location because both the top and bottom side of each sample was machined so that the surfaces would be flat and parallel. Specimens were created so that the weld would be centered in the gage length and running perpendicular to the axial loading.

Digital image correlation (DIC) was used to measure the strain for the welded tensile test samples. This system required the application of a random speckle paint pattern to the front surface of the gage length. Two high resolution cameras were placed near the sample and pictures were taken with these cameras at certain time steps. The software supplied with the cameras was then able to calculate the strain in the samples by monitoring the distance that the speckle pattern distorted in each frame. This method was chosen since the strain in the sample may not be constant, due to the diffusion mixture of materials in the weld and heat affected zone (HAZ).

Data collected during the test was also used to generate stress-strain curves for the samples, which was used to produce mechanical properties for the weld section where the specimens were observed to fail. Applied stress was determined from the measured applied load divided by the initial sample cross-section. Strain calculations for samples extracted from Configuration 1 were performed with the digital image correlation software, while strain values for samples from Configuration 2 were acquired through an MTS extensometer, 634.12-E54. Stress-strain curves were used to determine elastic modulus (E), 0.2% offset yield stress (YS), and ultimate tensile strength (UTS). Due to the large variation in YS and E, the elastic modulus

could not be determined over fixed strain range. Instead each curve was plotted and the elastic modulus was determined through the initial linear portion of the curve. Once the modulus was calculated a parallel line with a 0.2% strain offset was calculated. The value of yield stress is the intersection of this parallel line and the stress strain curve. Ultimate tensile strength was recorded as simply the maximum stress recorded at any one point along the stress versus strain curve.

3.2.2. Hardness Measurements

Hardness measurements were made using macro Vickers hardness machines. Vickers hardness was used in this work since this measurement has been shown to be directly related to the yield strength of the material [8]. Measurements were performed using a Leco V-100-A2 bench top hardness tester. All measurements were performed with 5 kgf.

The bench top hardness tester uses a filar optical eyepiece to measure the diagonal length of the square shaped indentations. The average diagonal lengths was used to determine hardness by

$$HV_5 = \frac{2*P*\sin\frac{\theta}{2}}{d^2} \quad (3)$$

where P is the applied force in (5 kgf), d is the average diagonal length (mm), and θ is the angle between the faces of the pyramidal indenter (136^o). The average diagonal length was determined by averaging the two measured diagonals of a single indentation.

A series of hardness measurements were made in a line along the length of the sample perpendicular to the welding direction, so that a profile could be obtained that characterized the parent material, the heat affected zone, and the weldment material. To do this, the sample was secured to a slide table that was controlled with a calibrated dial that allowed the relative position to be controlled. Indentations were made in 2mm increments starting at a distance from the weld centerline (~35 mm) that would ensure the material being tested was virgin parent material.

3.2.3. Heating

Isothermal furnace heating was performed using a Blue M Electric furnace with a temperature range of 593^{o}C. Using a programmable PID controller, the furnace was maintained within +/- 0.5^{o}C. In this method the furnace was heated to a desired temperature, samples were then placed into the heated furnace and heated until the samples has normalized at the set temperature. A sacrificial sample was placed in the furnace each time with a thermocouple attached. This sample was used to signal when the test samples had normalized to the furnace temperature. Time measurement began after the specimens had reached the desired temperature level. This heating method imparted an average initial heating rate of 21^{o}C/min with a deviation of 5^{o}C/min. When the desired sample temperature had been reached, the test samples were removed and immediately water quenched. Hardness measurements were made immediately following the exposure.

3.2.4. Material

Two different weld sample configurations were tested in this research both configurations contained 6082-T6 extrusion that was welded with 5183 filler material. Both configurations were welded with the metal inert gas method (MIG). The differentiation of the samples is only in the geometry of the weld assembly. The thicker samples from weld Configuration 1, extracted from the geometry in Figure 15, have a parent material thickness of 7mm and were welded with a double pass weld. In addition there are four conductive paths at the weld location for heat to transfer out of the weld to the rest of the part. The samples extracted from weld Configuration 2 shown in Figure 16 have a parent material thickness of only 5mm and all of the welding thermal energy must pass through the two plates being welded. Additional heat paths are located 37 mm from the weld.

3.3. Results

A series of tensile tests were performed to determine the mechanical properties of welded sample including yield stress, modulus of elasticity, and ultimate tensile strength. These tests were performed on samples from the configurations in Figure 15 and Figure 16. The response of welded aluminum alloy mechanical properties was characterized in relation with Vickers hardness. To accomplish this characterization, flat tensile test samples were extracted from the weld configurations shown in Figure 15 and Figure 16. From Figure 15, eight samples were extracted for testing: two baseline runs, 150^{o}C, 250^{o}C, 300^{o}C, 350^{o}C, 400^{o}C, and 500^{o}C. Since the geometry of each weld configuration differed slightly, four samples were extracted from the configuration shown in Figure 16 for testing following exposures of 150^{o}C, 300^{o}C, 400^{o}C, and 500^{o}C.

3.3.1. Weld Configuration 1

3.3.1.1. DIC and Failure

Selected pictures of the DIC calculated strain fields for weld Configuration 1 and corresponding fractured samples are shown in Figure 18 through Figure 25.

Figure 18 shows that the strain in the 150^{o}C sample is nearly uniform until yielding, Figure 18 a and 18 b. After reaching the yield point, the strain field becomes much more varied with higher localized strain at several locations; Figure 18 c. The strain field appears to have two distinct bands of higher strain, one located at the near bottom of the calculated field and the other just a little above it. The two regions of higher strain, ~10%, are separated by a small region of small strain, ~2%. Closely examining the picture in Figure 18 c, it can be seen that the cracking and eventual failure of the samples happens below this calculated field. Figure 19 shows the

failure of the physical sample. Small amounts of necking can be seen on both sides of the failure. The actual failure itself was smooth and at an oblique angle to the surface.

Figure 20 a and 20 b contain DIC strain fields for 300^{o}C. These figures show that once again up to yielding the strain across the sample was near uniform in its distribution. The small region of non-uniform stress in the bottom left corner which appears in Figure 20 b, taken during the yielding portion of the curve, is caused by the formation of a crack. In Figure 20 c the deformation of the sample has become plastic and the field is once again non-uniform. Unlike at 150^{o}C, there are not two regions of higher strain. The red regions of high strain, ~15%, are all centered around forming cracks when examined under higher magnification. Figure 21 shows a closer look at the break of the 300^{o}C sample. This failure exhibits less necking than the 150^{o}C sample, and the fracture is much more jagged and propagated nearly perpendicular from the surface.

The DIC calculated strain fields for the 400^{o}C sample are shown in Figure 22. As with the two previous samples, 150^{o}C and 300^{o}C, the distribution of the strain is very uniform until after yielding; Figure 22 a and Figure 22 b. After the sample begins to plastically deform as seen in Figure 22c, the strain increases locally to nearly three times what the majority of the sample is experiencing (~3-4% strain). The forming cracks, where strain reaches in excess of 14%, are only found in the bottom portion of the image, but are distributed nearly equally across the face of the sample. Figure 23 displays an enhanced view of the fractured 400^{o}C sample. There is even less necking than the 300^{o}C sample and the fracture looks more like what was seen at 150^{o}C. The fracture is jagged across the surface, but is much smoother through the thickness than the 300^{o}C sample and propagated at an oblique angle from the surface of the sample.

The 500°C sample strain fields in Figures 24 a and 24 b are uniform during the initial loading through yielding, similar to that seen in all the previous samples. In Figure 24 c, it is seen that the strain distribution has become non-uniform, with some areas experiencing ~10% while most of the area is experiencing greater than 4%. Unlike the previous samples no cracks can be seen in the regions of higher strain. Also of note, the other examples all displayed high strains roughly three times greater than the majority of the area. In this sample, the ratio is down to between 1.5 - 2. Figure 24 c does share the two region strain distribution as seen in Figure 18 c, although the values are different. Figure 25 is a picture taken of the fracture of the 500°C sample. This fracture has more necking than the 400°C and looks much like the fracture seen in the 300°C sample; jagged with near perpendicular to the surface propagation.

3.3.2. Stress Strain Curves

Stress-strain curves for the two weld configuration are shown in Figure 26 a for Configuration 1 and Figure 26 b for Configuration 2. These were used to determine the mechanical properties of the samples.

3.3.2.1. Modulus

Determined modulus of elasticity values are provided in Figure 27 for welded samples heated to a range of temperatures with a zero minute time exposure. Since the welded sample was constructed using 6082-T6 plate and 5183 filler, both of which have a modulus of elasticity of 70 GPa, then the expected room temperature elasticity value should be 70 GPa [2,20].The average room temperature modulus of elasticity calculated in this research was equal to 69.4 GPa, which is less than a 1% difference. At 250°C, the modulus increases to 78.9 GPa, which is 14% higher than the room temperature value. At 300°C, the modulus decreases to 66.9 GPa 4.9%

below the room temperature value. The modulus remains at 68-64 GPa for temperatures of 300°C- 500°C

3.3.2.2. Yield Stress

The welded aluminum samples did not display an elastic-plastic tensile response, so an offset method was used to determine an equivalent yield stress. For this research a 0.2% strain offset yield stress was calculated for each sample; the 0.2% offset yield stress for samples heated to different temperatures with zero minute soak time are provided in Figure 28. From the data in Figure 28, 0.2% yield stress was not affected by increasing the exposure temperature. The initial average value of 146 MPa is 42% lower than the parent material value of 250 MPa – 260 MPa[20]. As the maximum exposure temperature increases, the variation from the initial value is within 11% at all the test points for Configuration 1.

3.3.2.3. Ultimate Stress

The ultimate tensile strengths are shown in Figure 29. The absence of one of the room temperature baseline values is due to a machine failure that stopped the tensile testing after yield, but before failure. The baseline value of 304 MPa, agrees well with the parent material value of 290 MPa – 310 MPa [20]. The residual values of ultimate tensile strength are within 5.7% of the room temperature value up to the 250°C test point. Between 250°C and 350°C, the residual value of ultimate tensile strength decreases by 18%. This is followed by a return to a near baseline value for samples heated to temperatures of 400 and 500°C.

3.3.3. Weld Configuration 2

3.3.3.1. Modulus

Configuration 2 displays a near linear decline in modulus of elasticity values (see Figure 27), from 150°C to 500°C. The 150°C value was 61.5 GPa, which is 18% lower than the modulus

of elasticity at the same temperature for Configuration 1. Configuration 2 samples lose 19% of their modulus of elasticity value by 500°C, with a value of 50.0 GPa. Modulus values for Configuration 1 are higher at all test points, with the closest test result being at 300°C where the difference is only 13%.

3.3.3.2. 0.2% Offset Yield Stress

In Figure 28, it can be seen that samples from Configuration 2 and Configuration 1 give the same yield stress values, ~140 MPa, up to 300°C. At 400°C, the yield stress decreased by 55% to only 62.6 MPa. Only a 10% decrease was observed in Configuration 1 over the entire range. At 500°C there is a slight recuperation of yield stress value, 17% higher than the Configuration 2 value at 400°C.

3.3.3.3. Ultimate Strength

The change in ultimate strength with temperature in Figure 29 for the samples from Configuration 2 is offset and more pronounced than the trend observed with Configuration 1 results. At 150°C and 300°C, the trend in the values was similar to Configuration 1 but about 22% lower at both points. The lowest value of ultimate tensile strength for Configuration 2 occurred at a test temperature of 400°C. This is 50°C higher than with Configuration 1 with a value of 129 MPa or 57% of the 150°C value. A gain of 32% in ultimate tensile strength is achieved by increasing the exposure temperature to 500°C. Configuration 1 experiences a gain at 400°C of approximately 29%. The largest difference in ultimate tensile strength was measured at 400°C, where the values for Configuration 1 and Configuration 2 were 56% different.

3.3.4. Hardness Measurements

The welded samples contained two different materials, 6082-T6 parent material and 5183 filler alloy in the weld. Each of these materials had a different thermal history and react

differently to thermal exposure. To ensure that accurate and appropriate hardness values were obtained, measurements were made as profiles. Moving from one side of the weld, crossing the heat affected zone and weld, before coming to rest at virgin parent material on the other side.

3.3.4.1. Configuration 2

To measure the effect of exposure temperature on welded aluminum, 76.2 mm long rectangular samples were extracted from the geometry shown in Figure 17 a. The weld was centrally located in this coupon sample. Since the weld is comprised of a heat treated alloy, 6082-T6, and a non-heat treated alloy, 5183 filler material, the hardness profile across the weld should change with exposure temperature. For Configuration 2 Figure 17a shows that at room temperature and 150^{o}C that the hardness of the parent material is substantially higher than the hardness at the weld centerline. The asymmetrical shape of the profile is caused by the use of two welding passes which are not concentrically applied. Therefore, one side of the weld experiences a higher heat input than the other. The side with the lower parent material hardness was the side that the second weld pass biased towards.

As the maximum exposure temperature is increased, the parent material loses hardness. The weld itself, comprised mainly of 5183 filler alloy, loses almost zero hardness values as the temperature is increased. Because the weld changes negligibly with exposure temperature and the parent material changes substantially, a crossover temperature is experienced. This crossover occurs when the parent material, which started with a higher hardness value, becomes softer than the weld material. Using the coupon samples to determine this temperature yields a maximum exposure temperature between 250^{o}C and 300^{o}C as the point where this crossover occurs. The minimum hardness for the parent material occurs at the 400^{o}C test point, where the weld hardness is nearly double that of the parent material. At the final test temperature of 500^{o}C, the

parent material gains significant hardness to the point where the 6082-T6 parent material and the 5183 weld material hardness values were within 8%.

As exposure temperature increases the profiles become much more symmetrical and uniform. Looking at the room temperature baseline profile the left side (locations less than 0 mm) is nearly 20 HV_5 higher than the right side. By 300°C, the two sides have become nearly identical. The increase in exposure temperature also seems to normalize the parent material, the variation between adjacent measurements declines as the temperatures increases.

3.3.4.2. Configuration 1

The trend seen in Figure 17b is evident in the tensile test specimens from Configuration 1, although the degree to which the exposure temperature affects the hardness values seems to be diminished. The baseline profile exhibits higher hardness values in the parent material than found in the weld region; the weld being 12 mm across and the HAZ extending approximately 18 mm from the weld centerline. The Vickers hardness outside of the heat affected region diminishes slightly as exposure temperature increases, and the 5183 alloy found in the weld displays less than 6% change in residual hardness values as temperature increases. The critical temperature seen in Figure 17 a, between 250°C and 300°C, is not observed in the data from the tensile samples, Configuration 1. Instead the 6082-T6 parent material exhibits a higher residual hardness value until the 400°C exposure temperature is achieved. For the 400°C and 500°C profiles, the residual hardness values between the parent material and weld material are within 12%.

3.4. Discussion

3.4.1. Effect of Exposure Temperature

Exposure temperature causes minimal changes in samples extracted from Configuration 1. Yield stress for instance displays results within 6% of the initial value at all test points. Ultimate tensile stress shows a significant decrease at only two temperatures, 300^{o}C and 350^{o}C, before returning to a value near the baseline value. The modulus of elasticity shows some increases as the temperature first increases (Figure 27), but at 300^{o}C it displays a value near the room temperature for the rest of the test temperatures. This indifference to exposure temperature can be supported by viewing the stress-strain curves in Figure 26 b; the curves almost lie right on top of each other at all temperatures. The similarity of material properties at all temperatures is attributed to the weld geometry. All the heat must either radiate from the surface or conduct through the parent material. The low yield stress and ultimate tensile stress values may be an artifact of the weld geometry. Since the welding requires substantial heat input and Configuration 1 has limited paths for the thermal energy to evacuate the weld material further from the weld may have experienced temperatures that already affected the material properties.

By examining Figure 26a, it can be seen that the samples extracted from Configuration 2 respond much more to an increase in exposure temperatures. The stress-strain curves do not lie on top of each other, demonstrating that exposure temperature alters the mechanical properties. Because of the geometry seen in Configuration 2; heat input from the weld can conduct through several paths. Since the heat is more effectively dissipated, the surrounding material is not expected to reach as high of temperatures as does the material in weld Configuration 1. Without being exposed to elevated temperatures previously, the material is affected much more dramatically by being heated.

3.4.2. Relationship of Hardness and Weld Failure Location

Table 2 lists the break locations of samples from weld Configuration 1 along with the local hardness at this break location. All of the breaks happened within 4 mm of the weld centerline. With the weld being approximately 12 mm across at the surface all of the fractures occurred within the weld itself. Since the parent material shows only a slightly higher value than the weld in Figure 17 b, failure could be expected in the welded zone due to the heating effects imparted by the welding process. Four tensile tests done on samples from Configuration 2 all fractured just outside of the weld; although no quantitative values were recorded. Examining the gross amount of difference between hardness values of the parent material compared to the weld filler material in these samples, a fracture outside of the weld would seem likely.

3.5. Summary of Findings

Exposure temperature affected both the hardness profiles for both the samples from configuration one and configuration two in the same manner. As the temperature rises beyond 150^{o}C the virgin parent material hardness decreases with each increase in temperature. Most noticeable in Figure 17a, a critical temperature can be extracted from the data. Between 250^{o}C and 300^{o}C the hardness value of the parent material drops below the value of the 5183 filler material. Analyzing the recorded mechanical properties at this temperature shows that yield stress is not significantly different, and modulus of elasticity sees only a very slight decrease. Ultimate tensile strength between these two points however is very different. Elevated temperatures above 150^{o}C have a detrimental negative effect on the hardness profile of 6082-T6 extrusion. By 250^{o}C the parent material has irreversibly been softened to a point below the 5183 weld filler material. Exposure to elevated temperatures does smooth out hardness recordings in samples, making the material much more homogenous.

As exposure temperature increases, discernible trends in sample failure were not found. Examining the values found in Table 2, it is clear that failure location does not change relative to weld centerline as exposure temperature increases. For the samples extracted from Configuration 1, elevated temperatures have a negligible effect on mechanical properties such as yield stress, modulus of elasticity, and ultimate tensile strength. Configuration 2 yielded samples that had increasing percent elongation as temperature rose to 300^{o}C, showing a more ductile trend for failure. This trend is supported by the decrease in modulus of elasticity and drops in both the yield and ultimate strength.

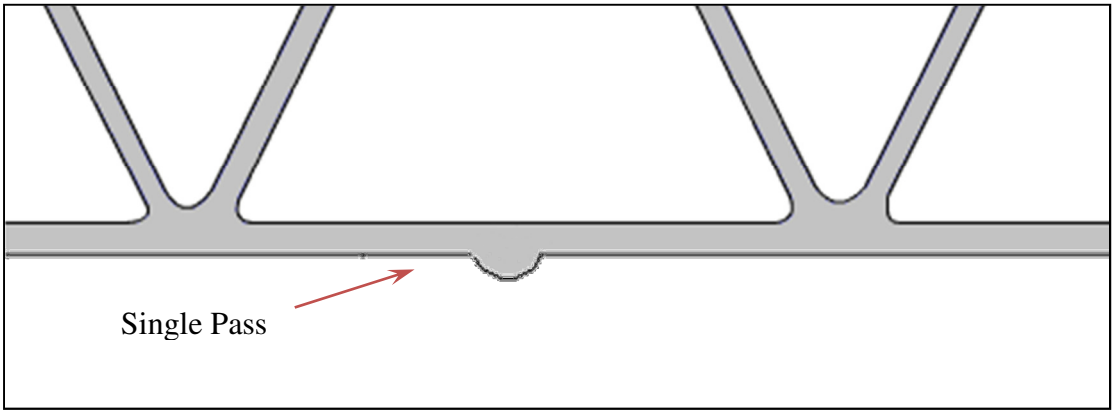

Figure 15 Weld Configuration 1[26]

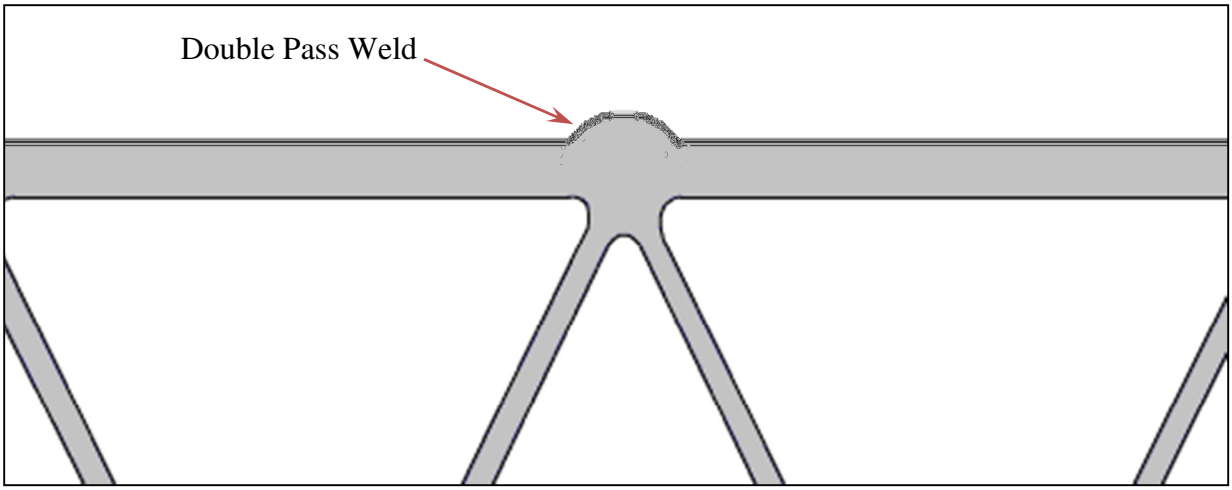

Figure 16 Weld Configuration 2[26]

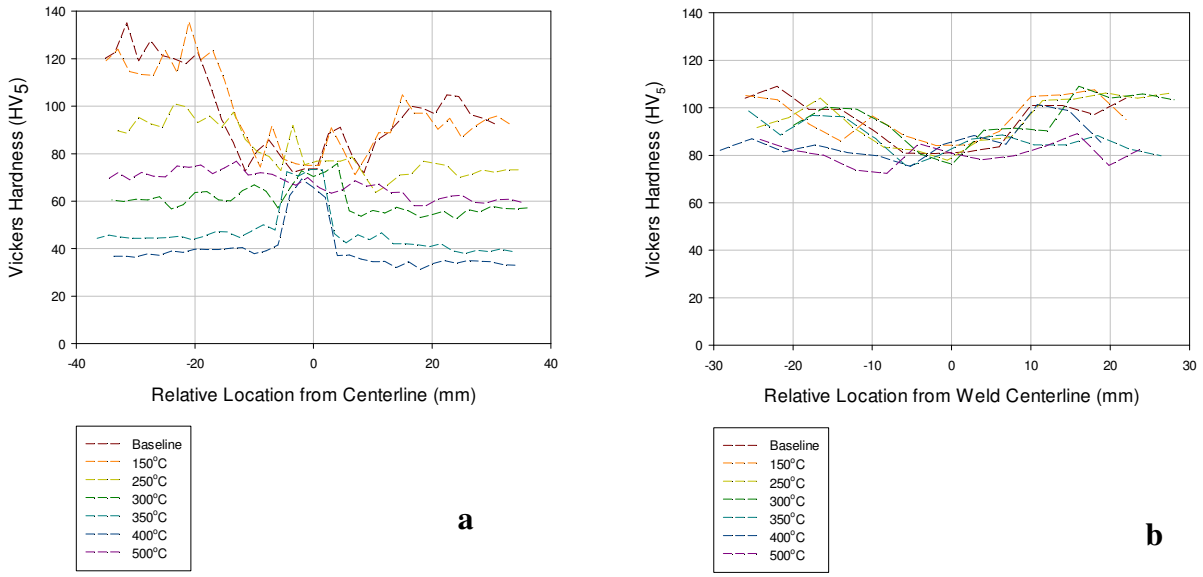

Figure 17 Hardness Profiles Across the Different Weld Geometries for (a) Configuration 2 and (b) Configuration 1

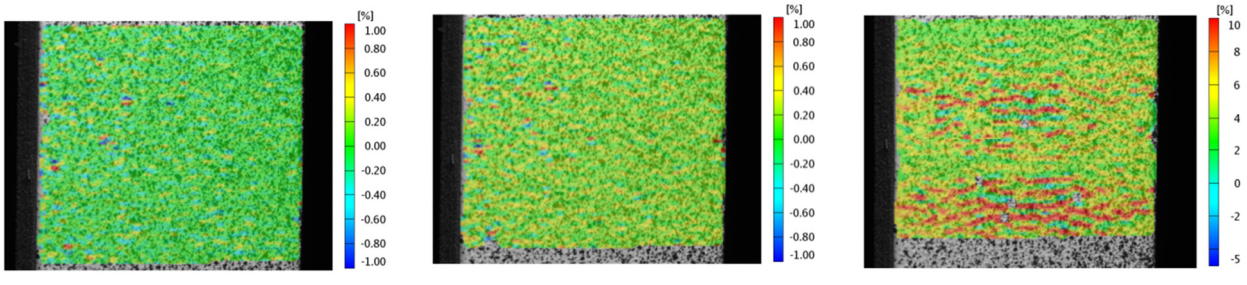

Figure 18 DIC Calculated Strain Fields for 150°C for (a) initial, (b) onset of yielding, and (c) prior to failure

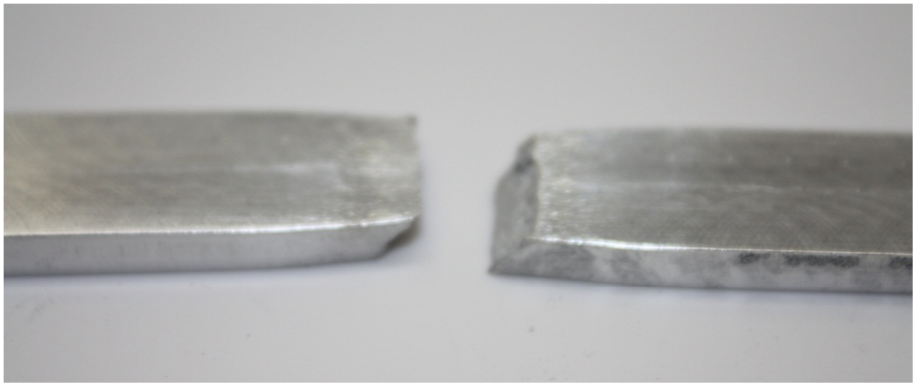

Figure 19 Failure Location of 150°C Weld Sample from Configuration 1

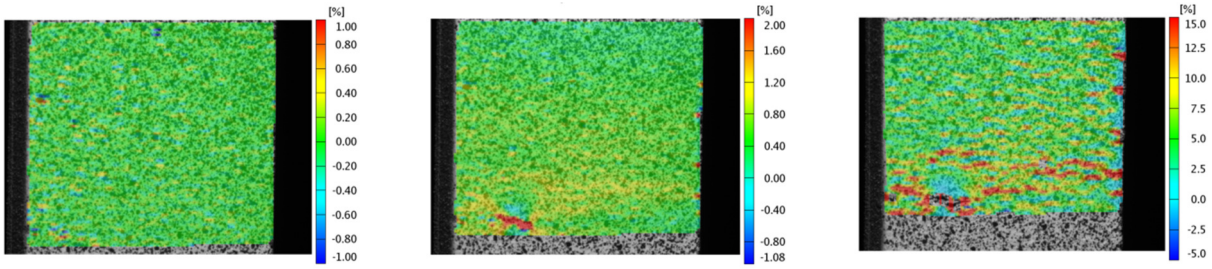

a B c

Figure 20 DIC Calculated Strain for 300°C Sample for (a) initial, (b) onset of yielding, and (c) prior to failure

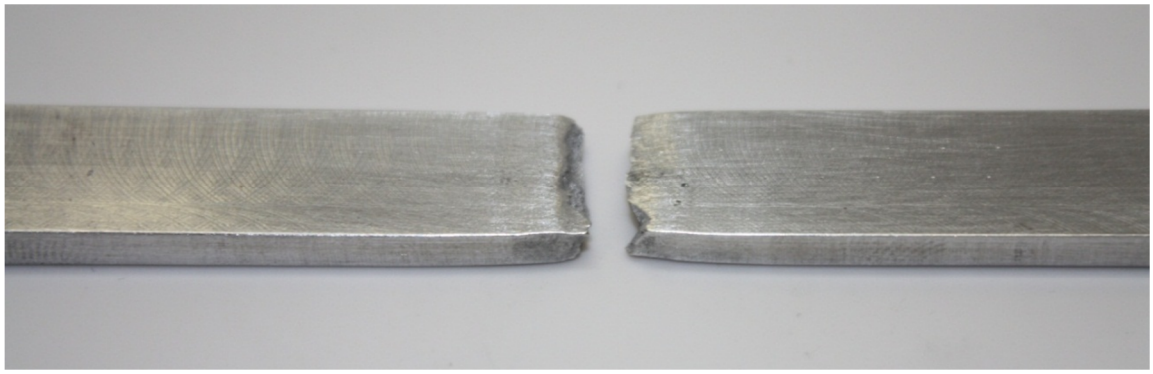

Figure 21 Break Location for 300°C Sample from Configuration 1

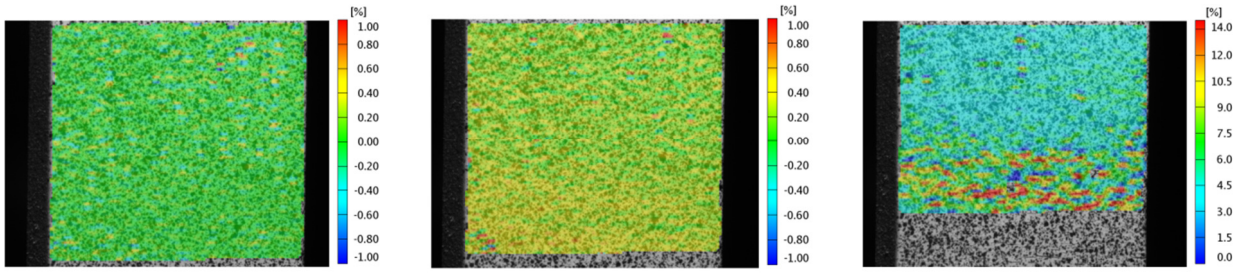

a B c

Figure 22 DIC Calculated Strain for 400°C for (a) initial, (b) onset of yielding, and (c) prior to failures

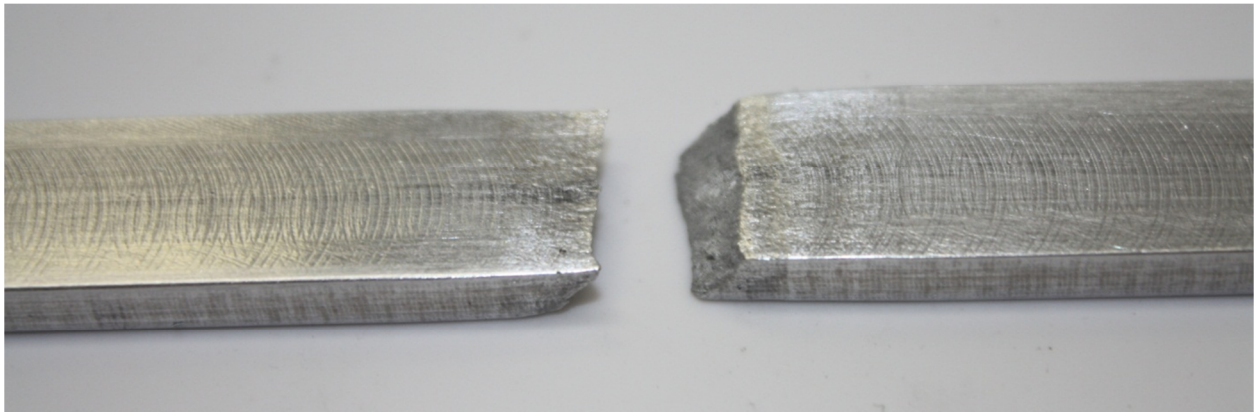

Figure 23 Break Location for 400°C Sample from Configuration 1

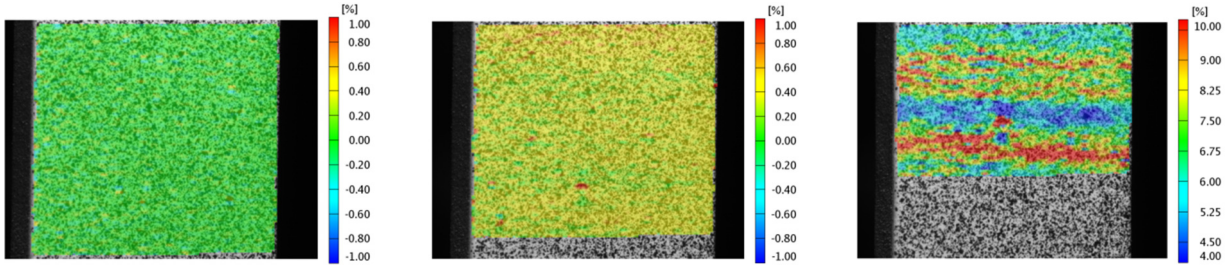

a B c

Figure 24 DIC Calculated Strain for 500°C for (a) initial, (b) onset of yielding, and (c) prior to failure

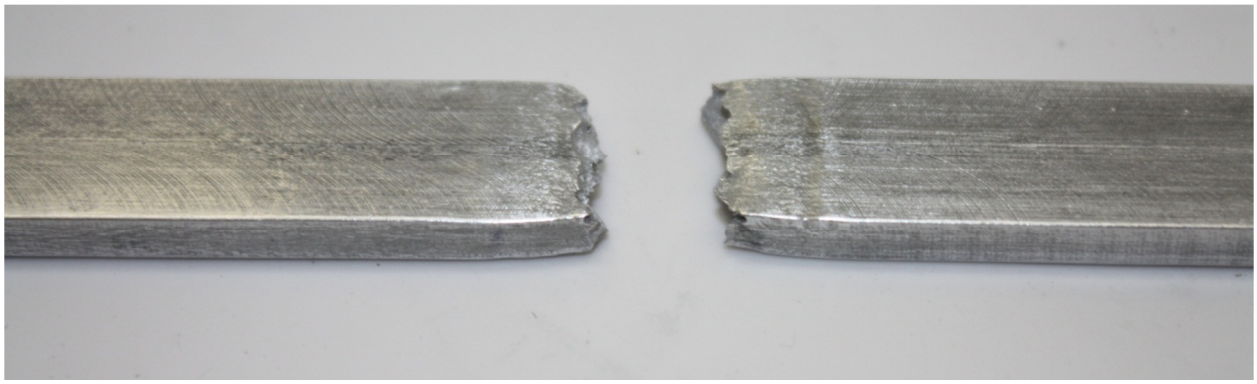

Figure 25 Break Location for 500°C Sample from Configuration 1

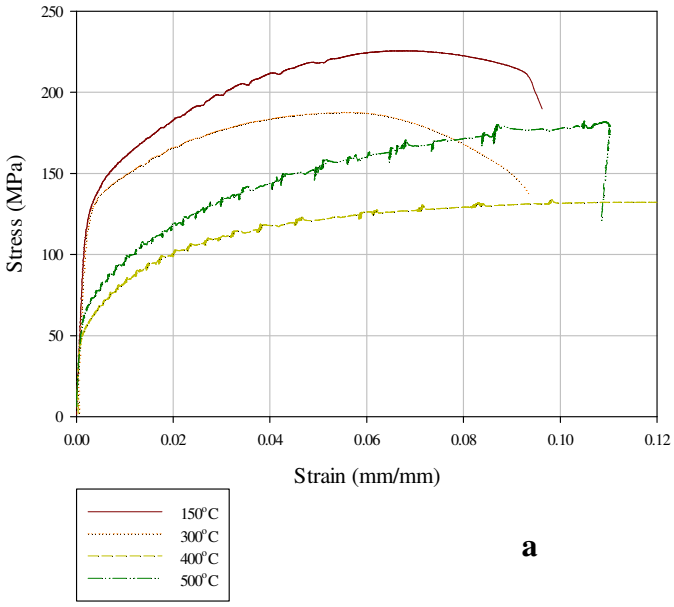

a

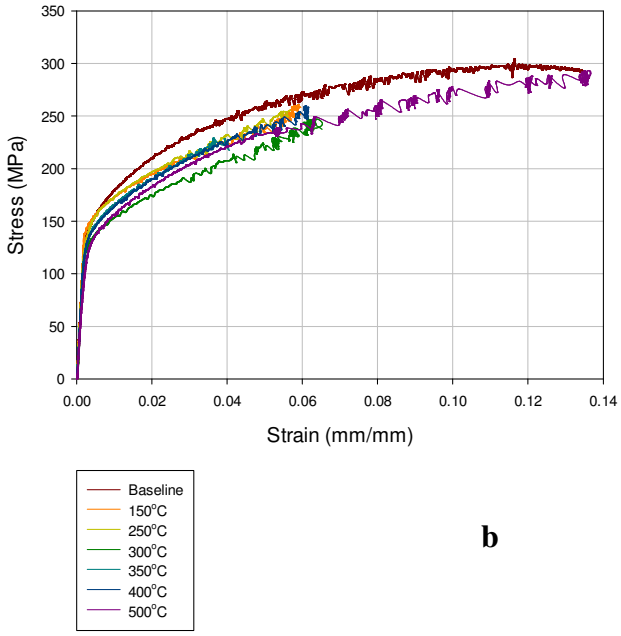

b

Figure 26 Tensile Test Results for the Different Geometries for (a) Configuration 2 and (b) Configuration 1

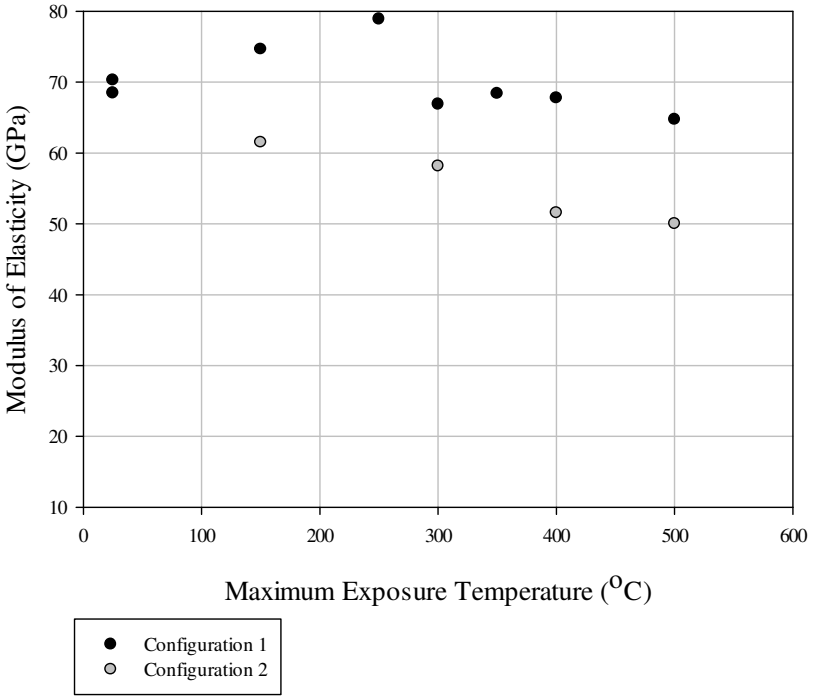

Figure 27 Modulus of Elasticity Results

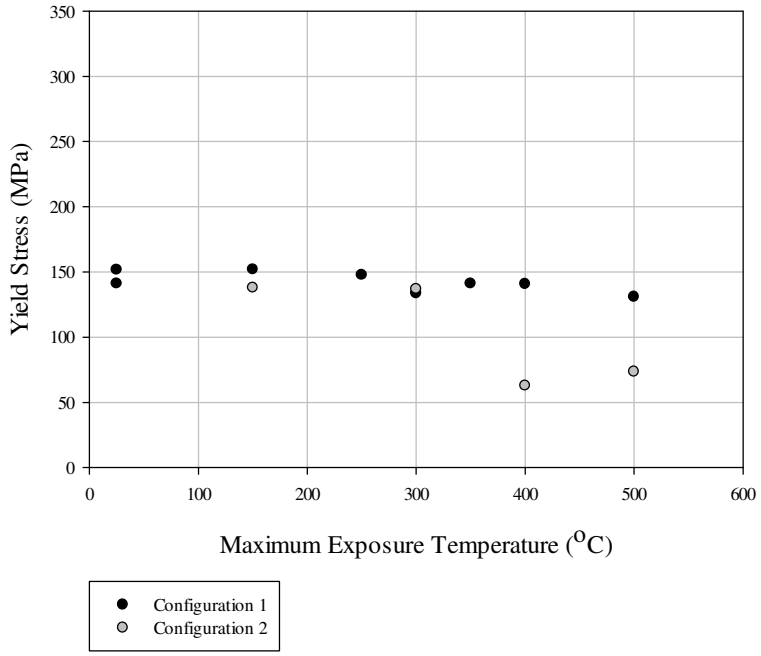

Figure 28 0.2% Yield Stress Results

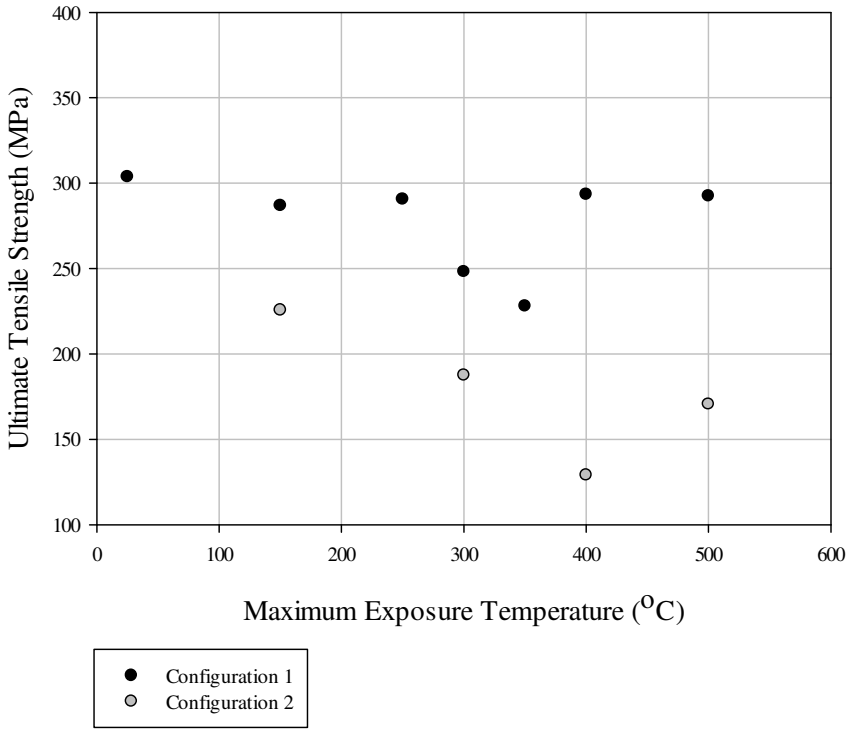

Figure 29 Ultimate Tensile Strength Results

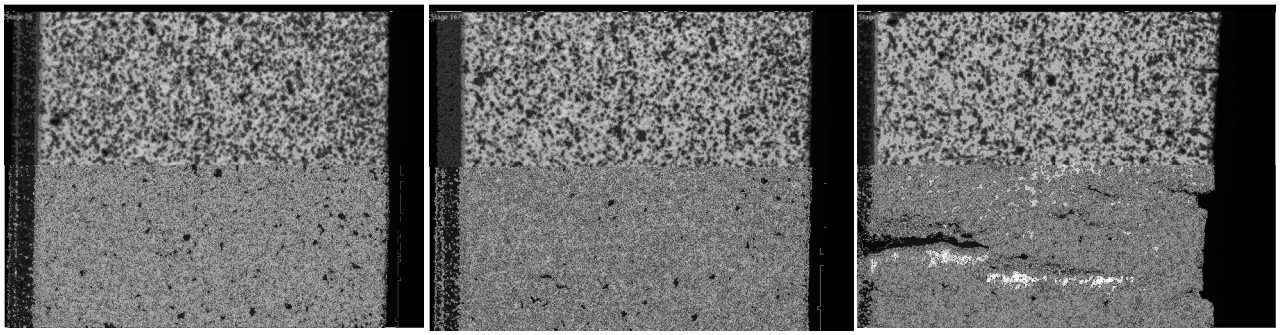

Figure 30 Digital Image Correlation Images for 300°C Test Sample Showing Progression of Failure

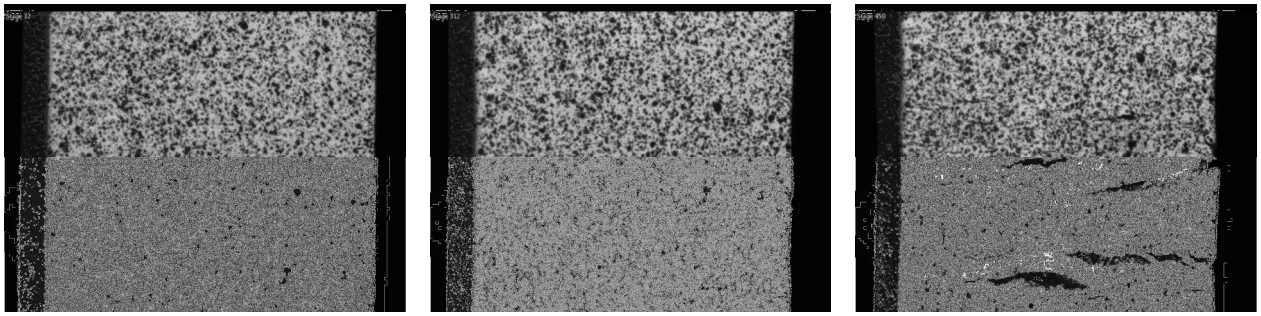

Figure 31 Digital Image Correlation Images For 400°C Sample Showing the Progression of Failure

Table 2 Break Locations and Interpolated Hardness Values

Sample	Location Relative To Weld Centerline (mm)	Location Hardness (Hv_5)
Baseline	-0.02	
150°C	-3.98	86.2
250°C	-3.32	80.8
300°C	2.07	83.3
350°C	0.41	83.3
400°C	-3.17	79.8
500°C	-2.88	83.6

4. CONCLUSIONS

The growing replacement of steel structures with aluminum alloy structures presents many opportunities and challenges. A comprehension of the permanent effects of fire exposure on aluminum alloys must be fully understood to maximize the benefits of using aluminum alloys. This thesis presented the response of two aluminum alloys to elevated temperatures; utilizing several heating methods and a variety of soak times.

The mechanical properties of aluminum alloys were strongly dependent on their family; the 5083-H116 and 6082-T651/T6 extrusion alloys displayed different responses to temperature increases. For 5083-H116 materials the loss in Vickers hardness was much more subtle than for 6082, showing a near linear decline from the room temperature values to rest at the annealed state. In the 6082-T6 alloys losses did not occur until after 150^{o}C, where over-aging begins to coarsen the precipitates. The drop in properties was most evident between 250^{o}C and 400^{o}C where the material becomes fully annealed from the T-6 state. Minimal property recovery was witnessed at the 500^{o}C test location, as a result of the beginning of solution heat treating the alloy. The welded 6082-T6 alloys displayed trends closer to the 5083-H116; slight variations as exposure temperature increases. This is the direct result of the heat input used for welding creating a heat affected zone where the material has near annealed mechanical properties.

The relationship of Vickers hardness to yield stress, as described by Tabor, does not trend well with aluminum alloys [7]. The non-linear shape of the tensile curves produced by both the 5083-H116 and 6082-T6 alloys required that a strain offset stress be calculated. The strain offset as determined by indenter size was 8%; this created a relationship between Vickers hardness results and stress with acceptable agreement. The use of 8% strain offset stress bears little usefulness in design calculations, so a relationship between Vickers hardness values and ultimate tensile strength values was computed. This resulted in a linear trend that matched the equation set forth by Tabor with adequate agreement and more useful than an arbitrary offset strain value for stress.

Particularly in welded samples, the viability of using a physical predictor such as Vickers hardness to assess material properties is minimal. While the hardness profiles measured changes in the relative hardness of the virgin parent material compared to the weld material, failure location fluctuated very little. Break location did not show an affinity to propagating from the lowest recorded values Vickers hardness. Due to the complex nature of welds, solely using Vickers hardness to try and assess the state of material properties is not sufficient.

REFERENCES

[1] Bray J. W. ;(Reynolds M. C., 2004, "Aluminum Mill and Engineered Wrought Products: Properties of Wrought Aluminum Alloys," ASM International Handbook, **2**, pp. 1-19.

[2] 2007, "Eurocode 9: Design of Aluminum Structures," pp. 1-60.

[3] 2004, "Heat Treating of Aluminum Alloys: Annealing," American Society of Metals Handbook, **4**, pp. 6-11.

[4] 2004, "Heat Treating of Aluminum Alloys: Strengthening by Heat Treatment," American Society of Metals Handbook, **4**, pp. 1-57.

[5] Maljaars J., Soetens F., and Snijder H. H., 2009, "Local buckling of aluminium structures exposed to fire. Part 1: Tests," Thin-Walled Structures, **47**(11), pp. 1404-1417.

[6] Maljaars J., Twilt L., and Soetens F., 2009, "Flexural buckling of fire exposed aluminium columns," Fire Safety Journal, **44**(5), pp. 711-717.

[7] Tabor D., 1951, The Hardness of Metals, Clarendon Press, London.

[8] Tabor D., 1954, "Physical Meaning of Indentation Hardness," Sheet Metal Industries, **31**(329), pp. 749-757.

[9] Tabor D., 1948, "A Simple Theory of Static and Dynamic Hardness," Proceedings of the Royal Society A: Mathematical, Physical and Engineering Sciences, **192**(1029), pp. 247-274.

[10] Maljaars J., and Soetens F., 2005, "Fire exposed aluminium structures," HERON, **50**(4), pp. 261-278.

[11] 2006, "Volume 03.01 Metals- Mechanical Testing; Elevated and Low-Temperature Tests; Metallography," Annual Book of ASTM Standards, ASTM International.

[12] Aginagalde A., Gomez X., Galdos L., and García C., 2009, "Heat Treatment Selection and Forming Strategies for 6082 Aluminum Alloy," Journal of Engineering Materials and Technology, **131**(4), p. 044501.

[13] Dadbakhsh S., and Karimi Taheri A., 2010, "Study on static strain aging of 6082 aluminium alloy," Materials Science and Technology, **26**(2), pp. 169-175.

[14] Topic, Irena; Hoppel, Heinz Werner; Goken M., 2008, "Influence of rolling direction on strength and ductility of aluminium and aluminium alloys produced by accumulative roll bonding," Journal of Materials Science (full set), pp. 7320-7325.

[15] 2006, "Volume 02.02 Aluminum and Magnesium Alloys," Annual Book of ASTM Standards, p. 811.

[16] Fogle, Emily J. ; Lattimer, Brian Y. ; Feih, Stefanie ; Kandare, Everson ; Mouritz, Adrian ; Case S. W., 2011, "Final Compression Load Failure of Aluminum Plates Due to Fire," Engineering Structures Journal (Submitted).

[17] 2004, "Properties of Wrought Aluminum and Aluminum Alloys: 5083 4.4Mg-0.7Mn-0.15Cr," American Society of Metals Handbook, **2**, pp. 64-66.

[18] Committee A. I. H., ed., 2010, "ASM Handbook, Volume 02 - Properties and Selection: Nonferrous Alloys and Special-Purpose Materials," ASM International Handbook, pp. 82-95.

[19] Committee A. I. H., ed., 2010, "ASM Handbook, Volume 02 - Properties and Selection: Nonferrous Alloys and Special-Purpose Materials," ASM International Handbook, pp. 96-108.

[20] 2008, "Aluminum and Aluminum Alloys - Extruded rod/bar, tube and profiles - Part 2: Mechanical Properties," British Standards Institution, London, pp. 1-66.

[21] Tekkaya A. E., 2001, "Improved Relationship Between Vickers Hardness and Yield Stress for Cold Formed Materials," Steel Research, **72**(8), pp. 304-310.

[22] Collette M., 2005, "Strength and Reliability of Aluminium Stiffened Panels By," University of Newcastle.

[23] Hartawan A., Thoe T. B., Ng S. T., Wu H., and Liu K., 2009, "Initial investigation into friction stir welding," SIMTech technical reports, **10**(1), pp. 5-9.

[24] Paik J. K., and Duran A., 2004, "Ultimate Strength of Aluminum Plates and Stiffened Panels for Marine Applications," Marine Technology, **41**(3), pp. 108-121.

[25] Pereira A. M., Ferreira J. M., Loureiro A., Costa J. D. M., and Bártolo P. J., 2010, "Effect of process parameters on the strength of resistance spot welds in 6082-T6 aluminium alloy," Materials & Design, **31**(5), pp. 2454-2463.

[26] Hoglund, Torsten; Soeten, Frans; Rothe, Jan; Hirsch, Jurgen; Rykeboer, Marc; Lundberg S., 2010, "Structural Design of a Movable Traffic Bridge I," aluMATTER.

APPENDIX 5083 – H116 A

5083 – H116 A

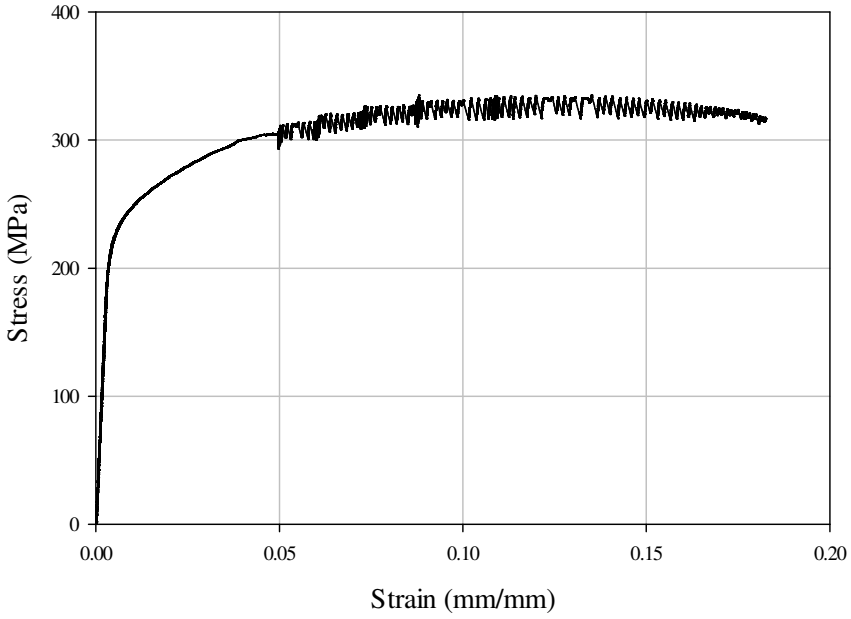

Baseline Zero Time		
Modulus of Elasticity =	65.18	GPa
Yield Stress =	228.18	MPa
Ultimate Tensile Strength =	333.77	MPa
HV_5 =	92.40	kg/mm^2
% Elongation at Failure	18.25	%

5083 – H116 A

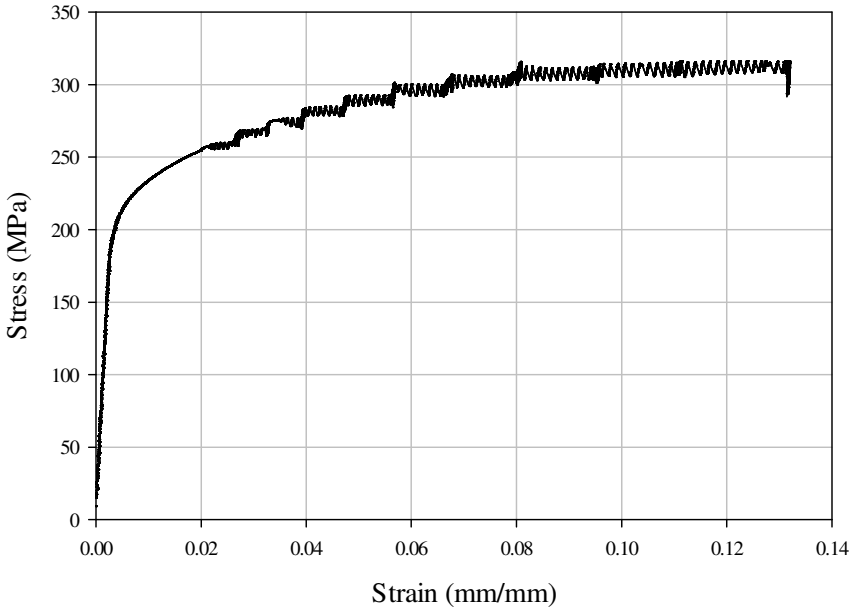

150°C Zero Time		
Modulus of Elasticity =	66.18	GPa
Yield Stress =	215.37	MPa
Ultimate Tensile Strength =	316.46	MPa
HV_5 =	97.88	kg/mm^2
% Elongation at Failure	13.20	%

5083 – H116 A

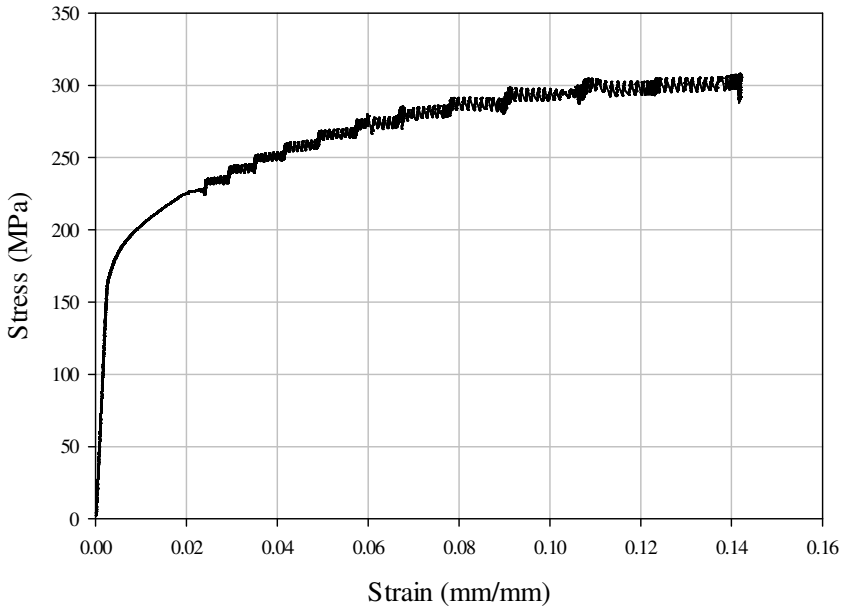

250°C Zero Time		
Modulus of Elasticity =	67.81	GPa
Yield Stress =	183.20	MPa
Ultimate Tensile Strength =	307.98	MPa
HV_5 =	89.08	kg/mm^2
% Elongation at Failure	14.22	%

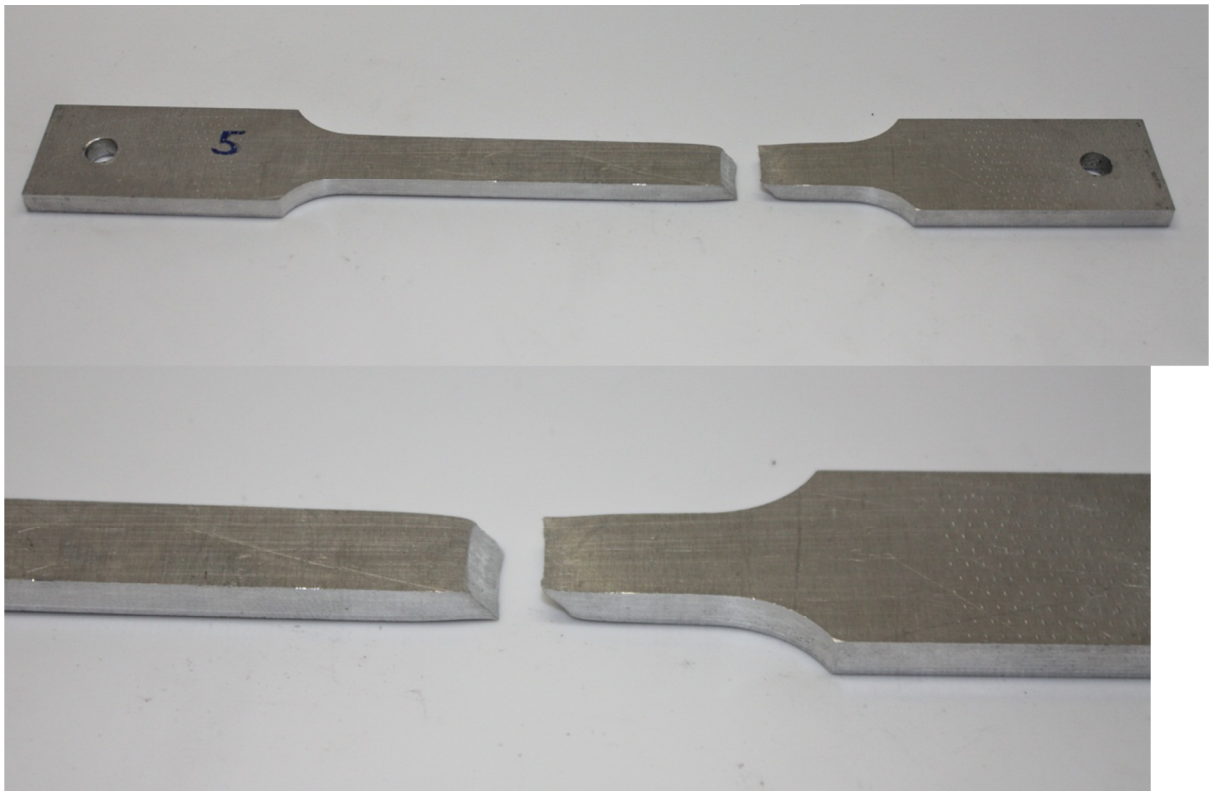

5083 – H116 A

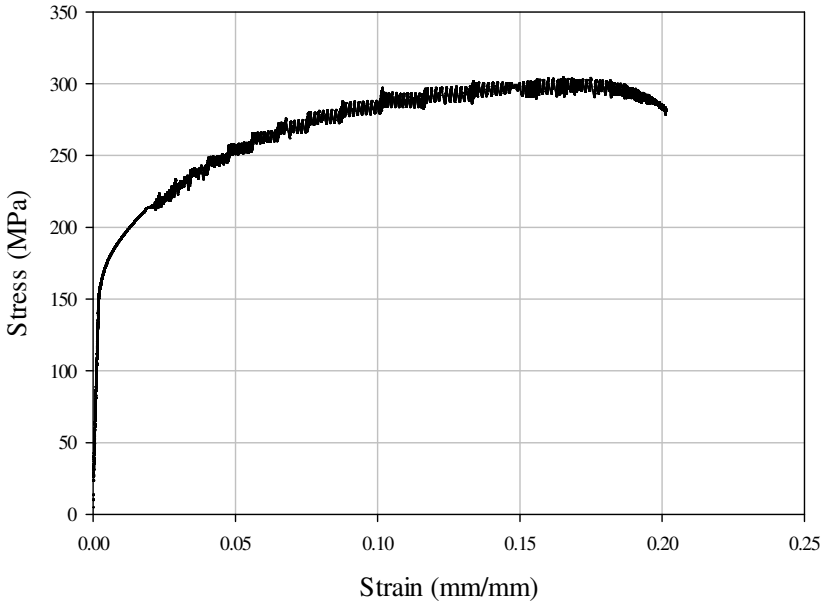

300°C Zero Time		
Modulus of Elasticity =	70.61	GPa
Yield Stress =	174.02	MPa
Ultimate Tensile Strength =	303.71	MPa
HV_5 =	92.37	kg/mm^2
% Elongation at Failure	20.13	%

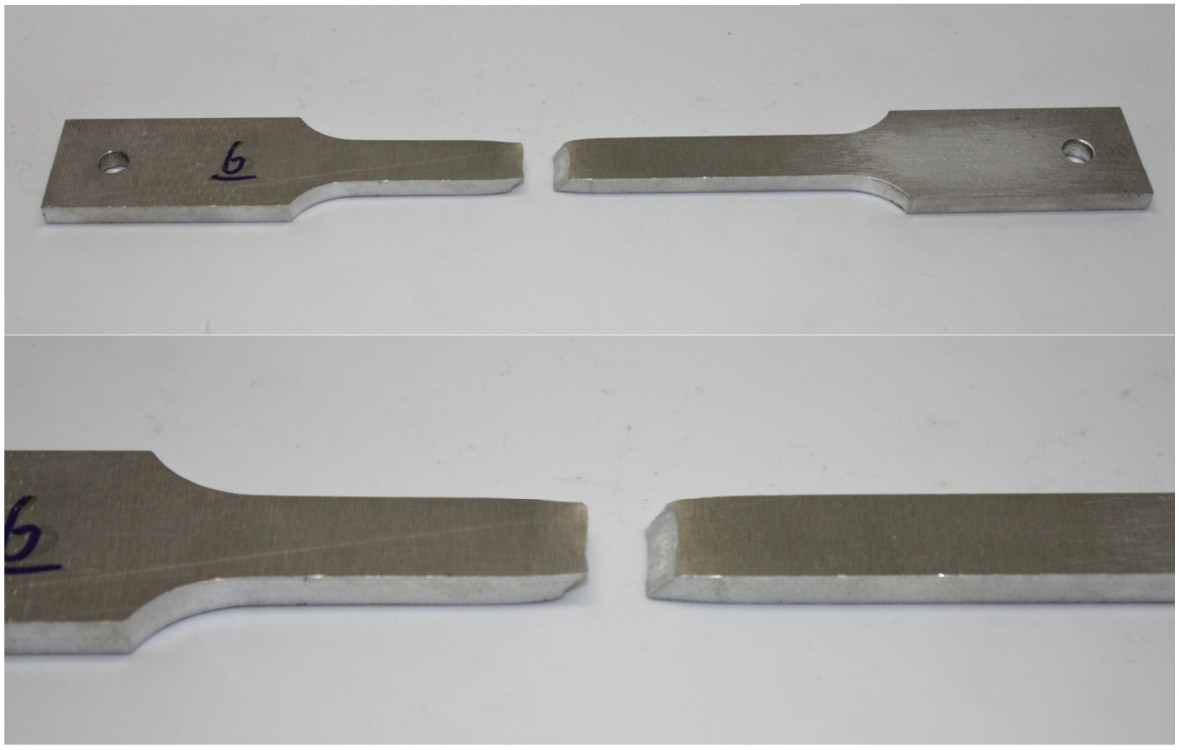

5083 – H116 A

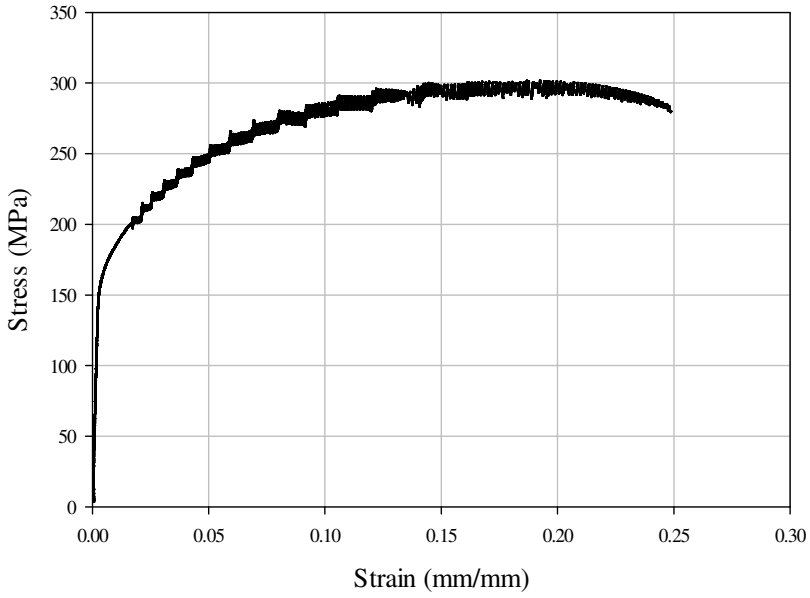

350°C Zero Time		
Modulus of Elasticity =	65.57	GPa
Yield Stress =	168.68	MPa
Ultimate Tensile Strength =	301.48	MPa
HV_5 =	87.12	kg/mm^2
% Elongation at Failure	24.86	%

5083 – H116 A

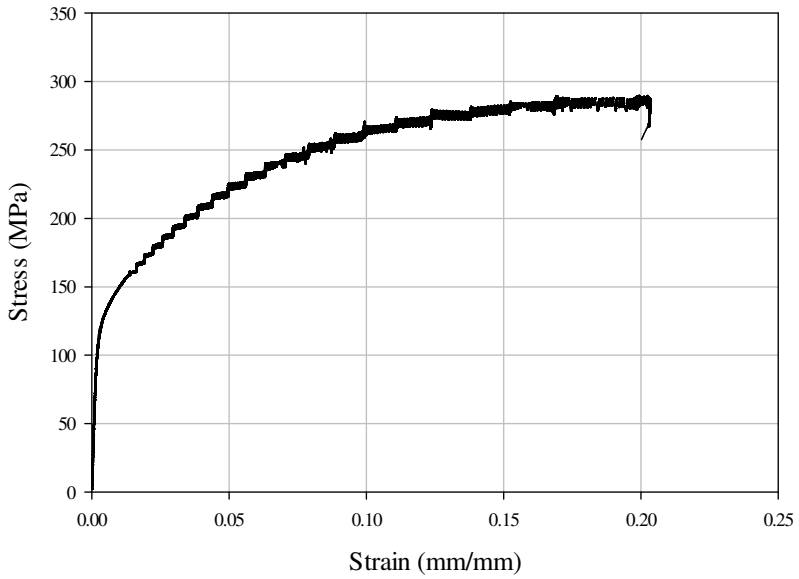

400°C Zero Time		
Modulus of Elasticity =	61.49	GPa
Yield Stress =	126.07	MPa
Ultimate Tensile Strength =	289.44	MPa
HV_5 =	77.25	kg/mm^2
% Elongation at Failure	20.33	%

5083 – H116 A

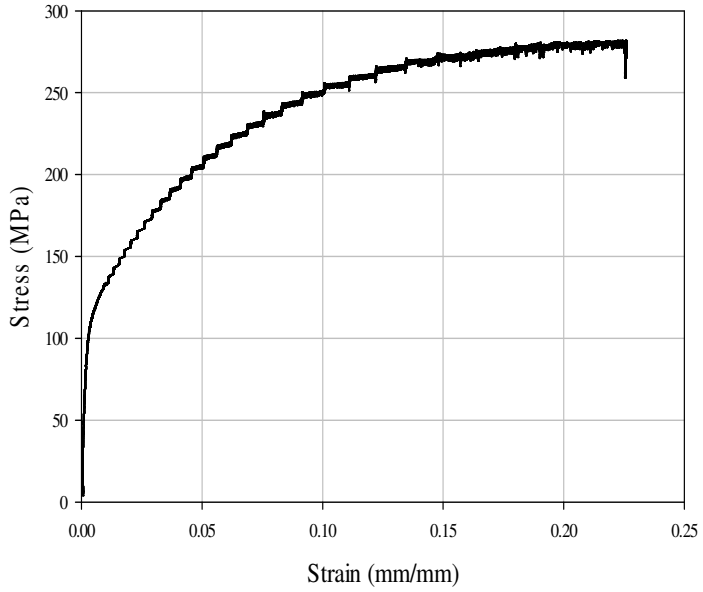
300
250
200
150
100
50
0
Stress (MPa)
0.00
0.05
0.10
0.15
0.20
0.25
Strain (mm/mm)


10

APPENDIX 5083 – H116 B

5083-H116 B

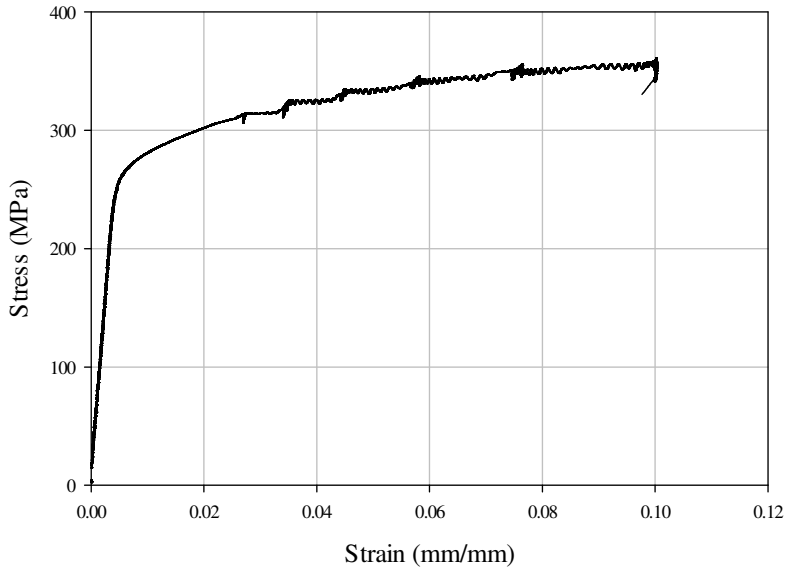

Baseline Zero Time		
Modulus of Elasticity =	58.82	GPa
Yield Stress =	269.35	MPa
Ultimate Tensile Strength =	360.76	MPa
HV_5 =	106.06	kg/mm^2
% Elongation at Failure	10.02	%

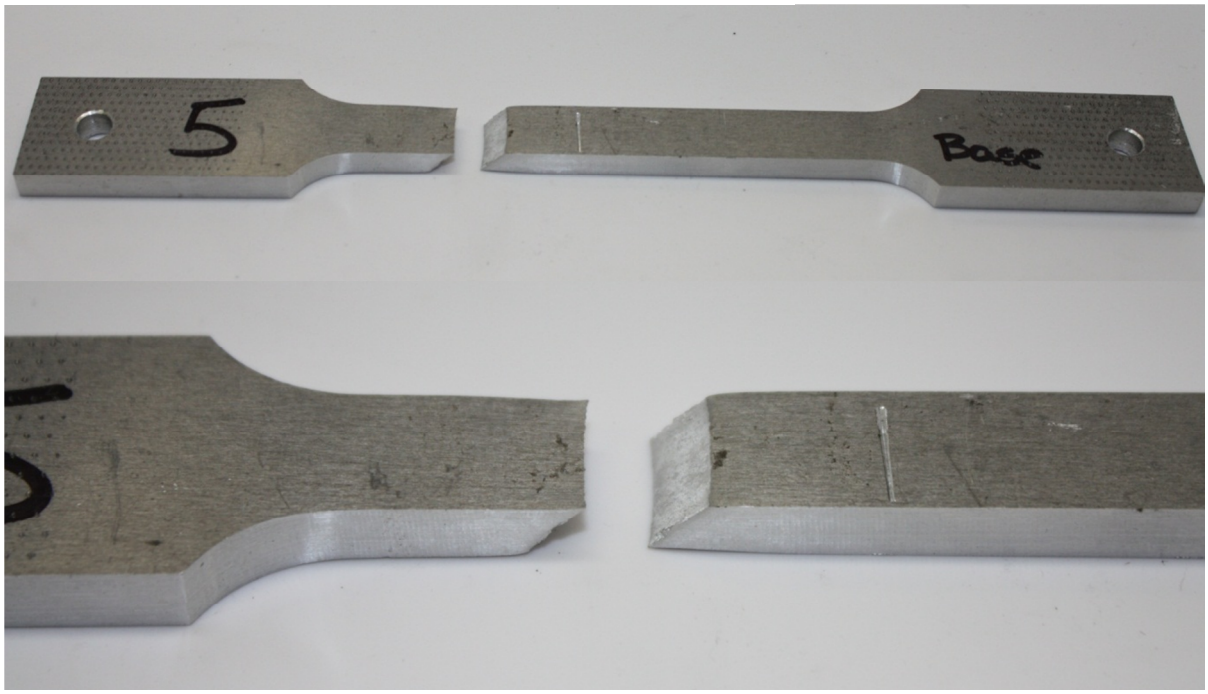

5083-H116 B

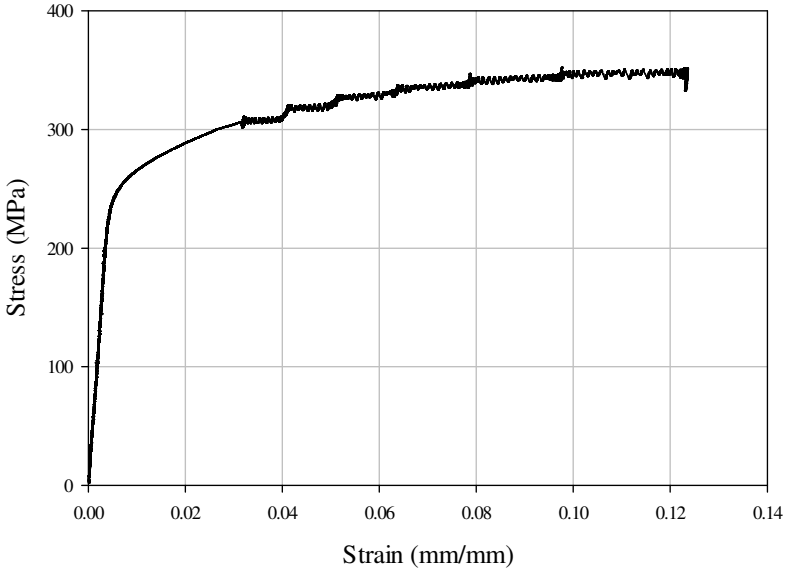

150°C Zero Time		
Modulus of Elasticity =	57.50	GPa
Yield Stress =	250.98	MPa
Ultimate Tensile Strength =	352.16	MPa
HV_5 =	104.63	kg/mm^2
% Elongation at Failure	12.35	%

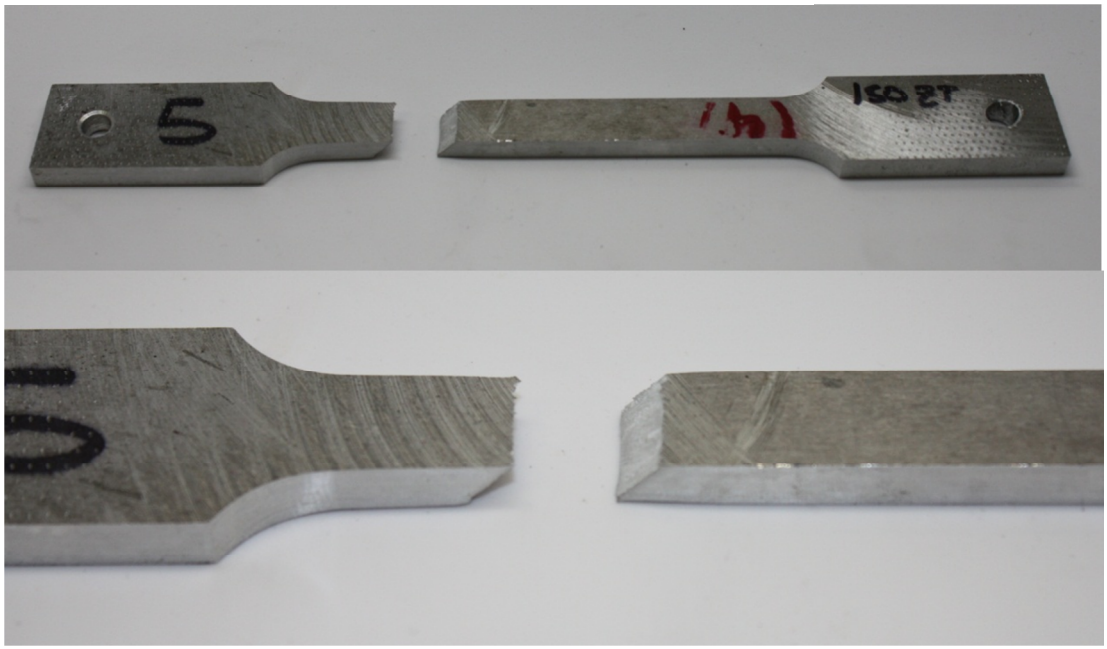

5083-H116 B

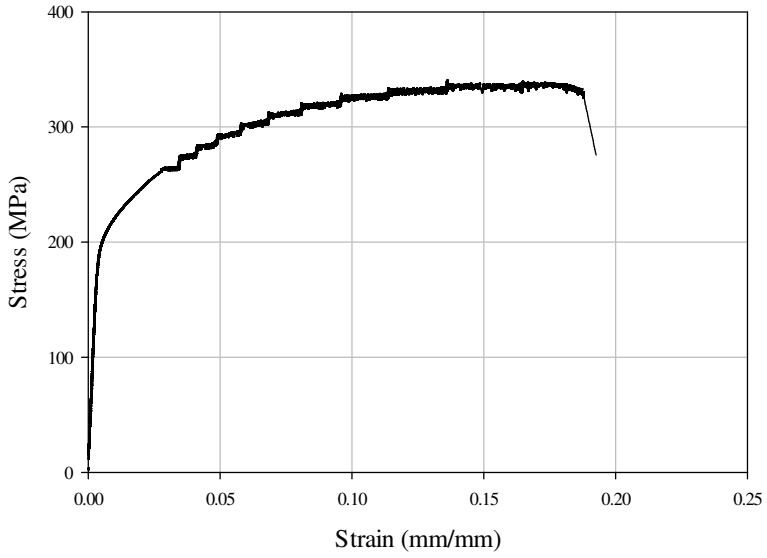

250°C Zero Time		
Modulus of Elasticity =	51.29	GPa
Yield Stress =	204.91	MPa
Ultimate Tensile Strength =	340.40	MPa
HV_5 =	94.75	kg/mm^2
% Elongation at Failure	19.27	%

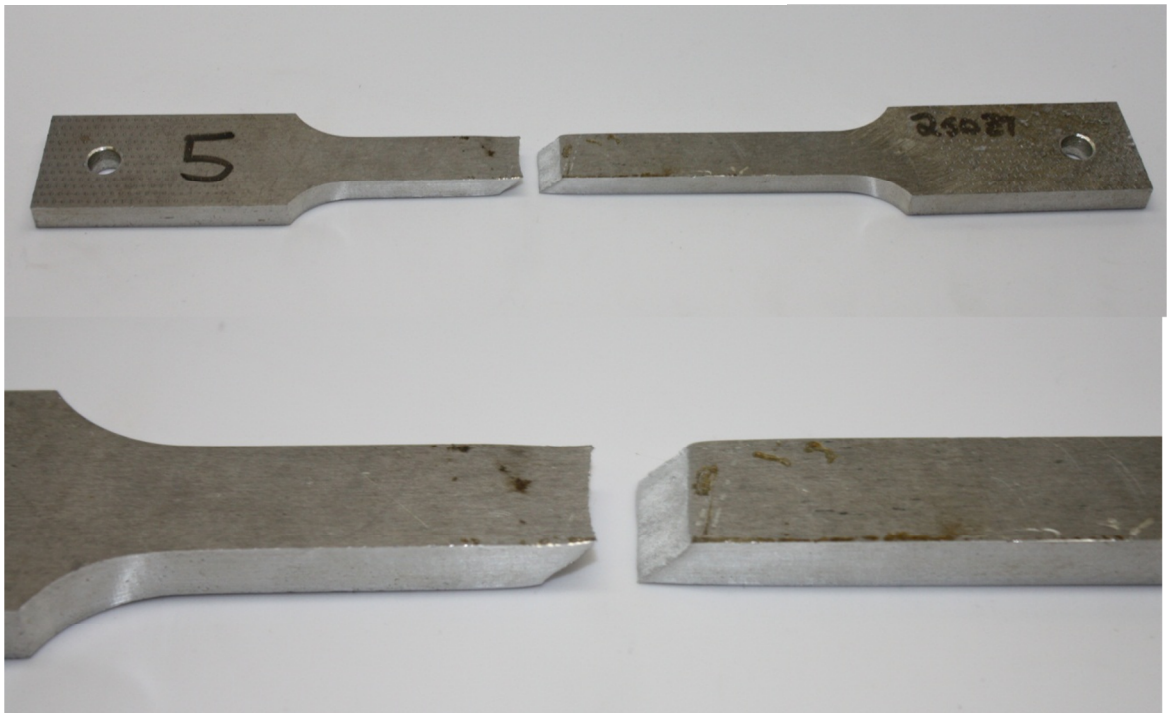

5083-H116 B

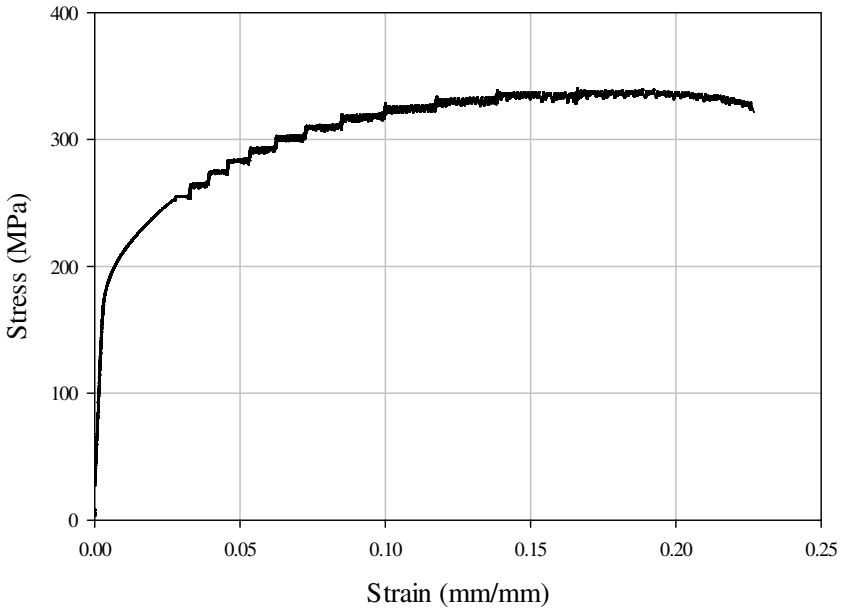

300°C Zero Time		
Modulus of Elasticity =	54.51	GPa
Yield Stress =	194.38	MPa
Ultimate Tensile Strength =	340.12	MPa
HV_5 =	95.28	kg/mm^2
% Elongation at Failure	22.69	%

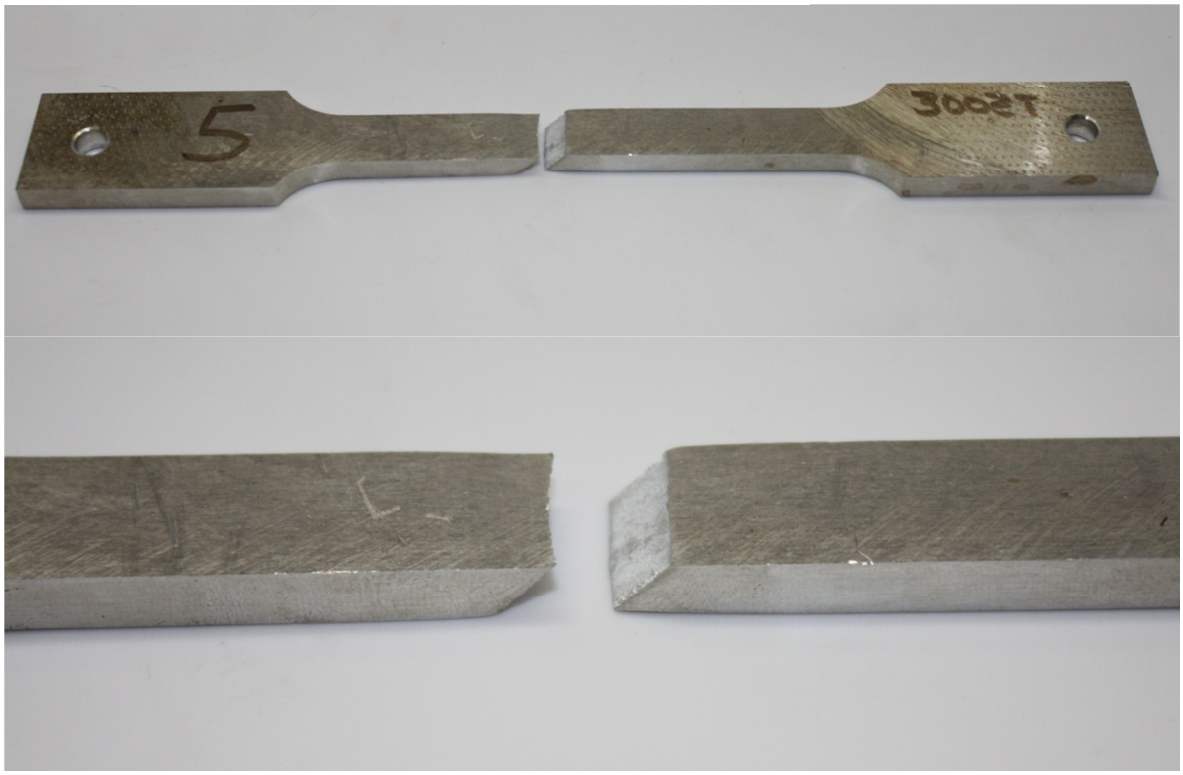

5083-H116 B

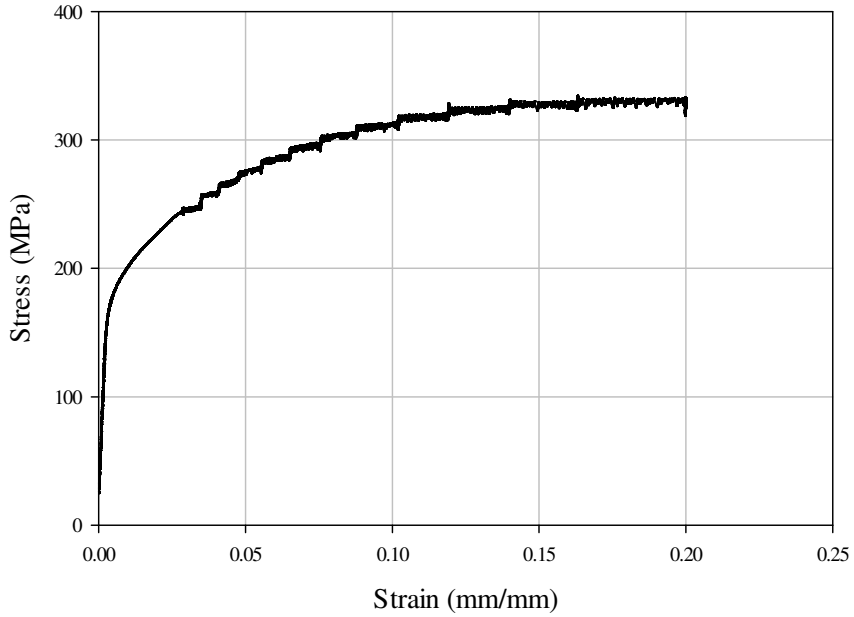

350°C Zero Time		
Modulus of Elasticity =	55.88	GPa
Yield Stress =	182.53	MPa
Ultimate Tensile Strength =	334.39	MPa
HV_5 =	87.63	kg/mm^2
% Elongation at Failure	20.01	%

5083-H116 B

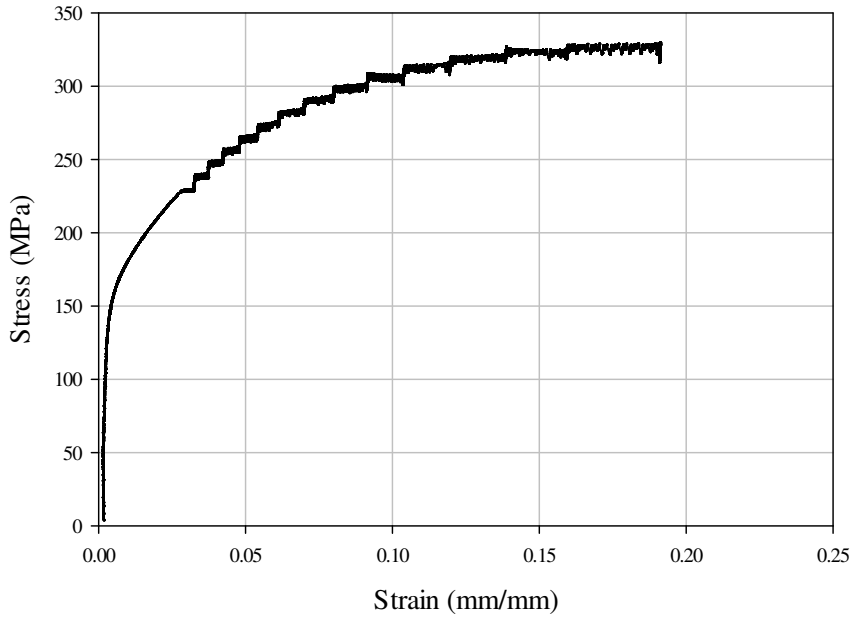

400°C Zero Time		
Modulus of Elasticity =	52.21	GPa
Yield Stress =	170.48	MPa
Ultimate Tensile Strength =	329.84	MPa
HV_5 =	84.69	kg/mm^2
% Elongation at Failure	18.98	%

5083-H116 B

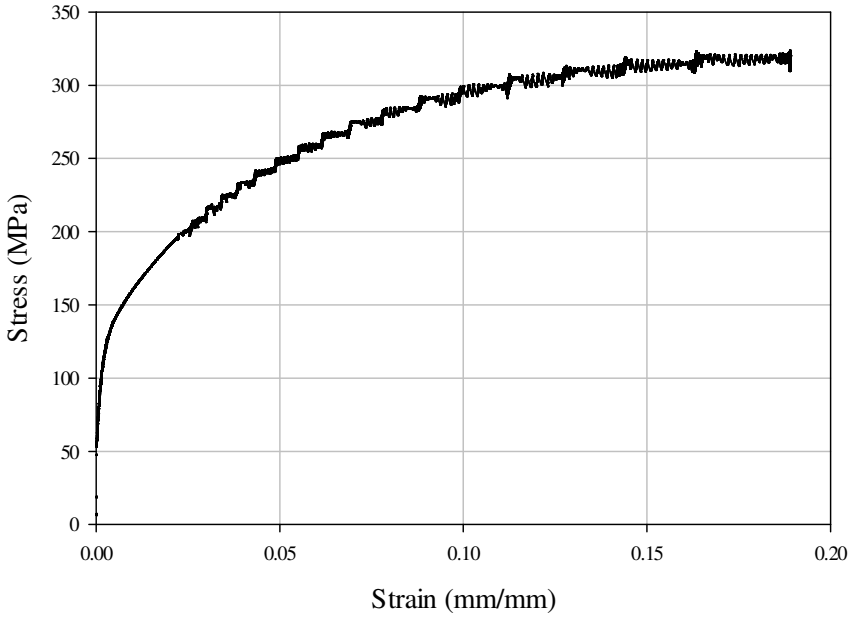

500°C Zero Time		
Modulus of Elasticity =	50.01	GPa
Yield Stress =	115.93	MPa
Ultimate Tensile Strength =	281.77	MPa
HV_5 =	73.21	kg/mm^2
% Elongation at Failure	22.58	%

APPENDIX 6082 – T651

6082-T651

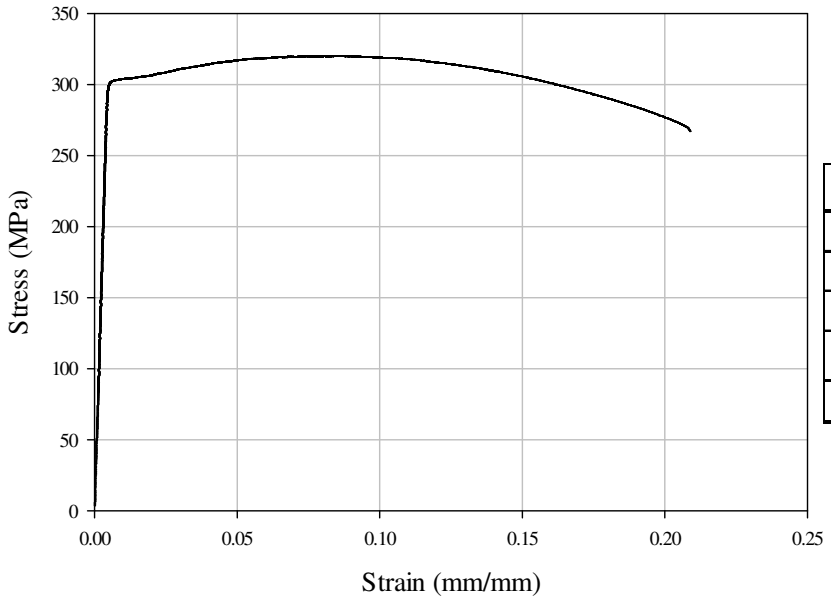

Baseline Zero Time		
Modulus of Elasticity =	68.69	GPa
Yield Stress =	302.34	MPa
Ultimate Tensile Strength =	289.40	MPa
HV_5 =	110.20	kg/mm^2
% Elongation at Failure	20.89	%

6082-T651

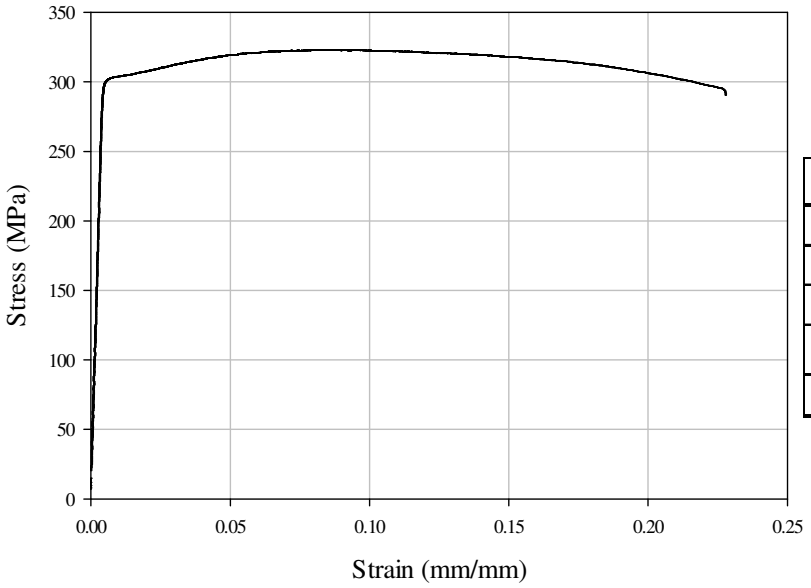

150°C Zero Time		
Modulus of Elasticity =	67.82	GPa
Yield Stress =	302.24	MPa
Ultimate Tensile Strength =	288.08	MPa
HV_5 =	111.89	kg/mm^2
% Elongation at Failure	22.79	%

6082-T651

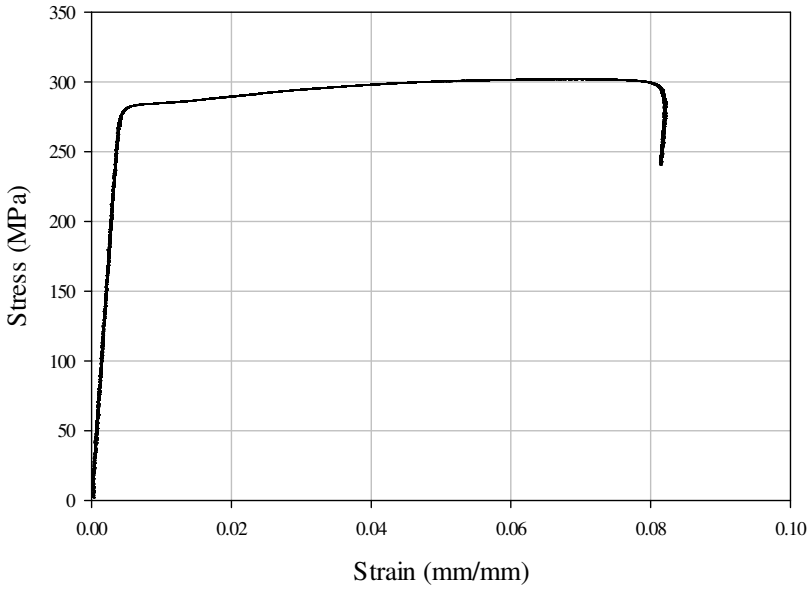

250°C Zero Time		
Modulus of Elasticity =	71.88	GPa
Yield Stress =	283.28	MPa
Ultimate Tensile Strength =	252.21	MPa
HV_5 =	105.39	kg/mm^2
% Elongation at Failure	8.22	%

6082-T651

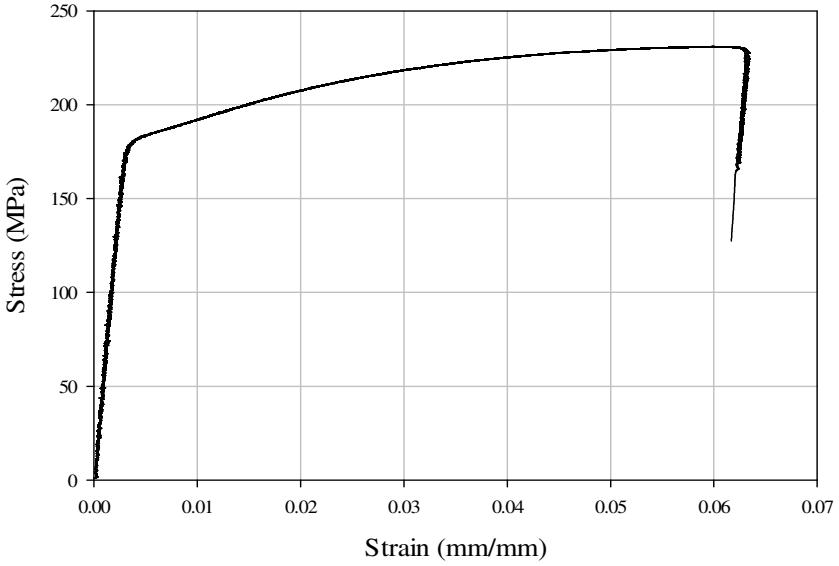

300°C Zero Time		
Modulus of Elasticity =	61.98	GPa
Yield Stress =	183.29	MPa
Ultimate Tensile Strength =	133.33	MPa
HV_5 =	79.48	kg/mm^2
% Elongation at Failure	6.33	%

6082-T651

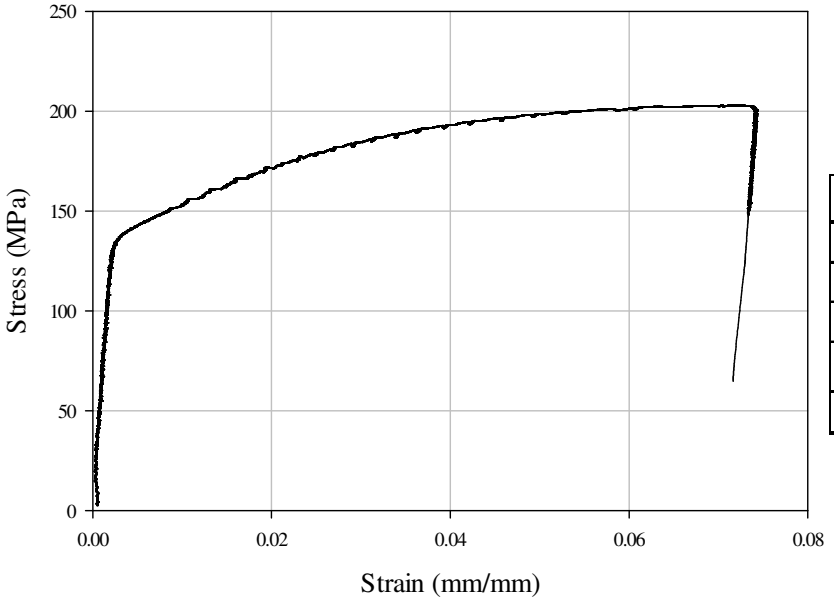

350°C Zero Time		
Modulus of Elasticity =	59.56	GPa
Yield Stress =	142.64	MPa
Ultimate Tensile Strength =	72.06	MPa
HV_5 =	64.27	kg/mm^2
% Elongation at Failure	7.38	%

6082-T651

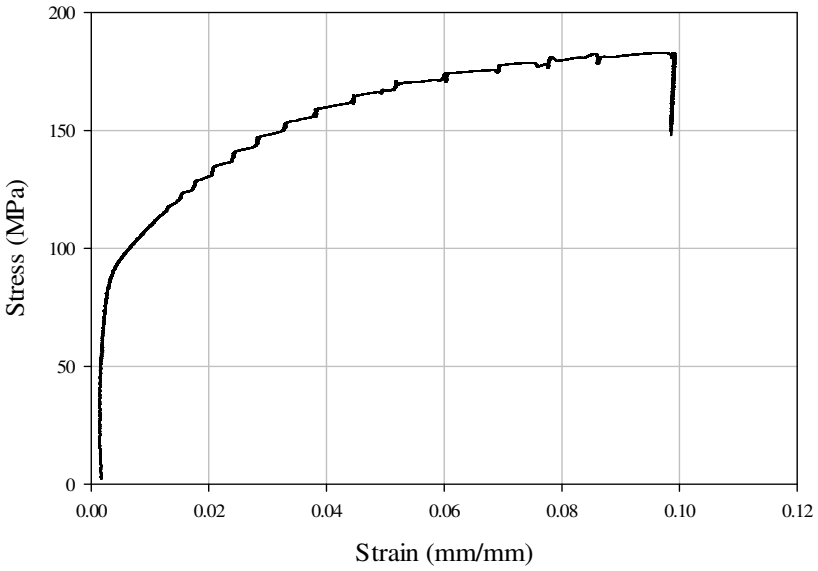

400°C Zero Time		
Modulus of Elasticity =	32.80	GPa
Yield Stress =	101.30	MPa
Ultimate Tensile Strength =	57.68	MPa
HV_5 =	57.88	kg/mm^2
% Elongation at Failure	9.75	%

6082-T651

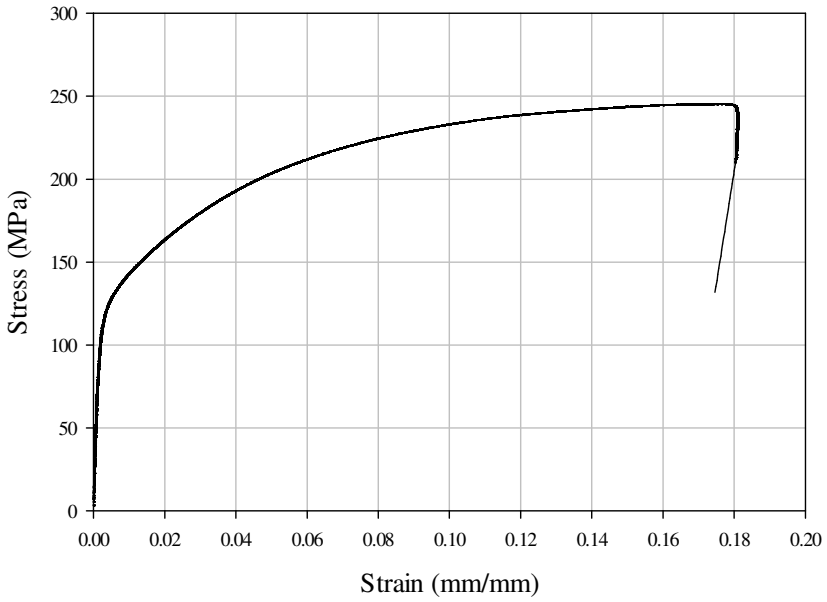

500°C Zero Time		
Modulus of Elasticity =	62.54	GPa
Yield Stress =	123.04	MPa
Ultimate Tensile Strength =	114.34	MPa
HV_5 =	68.43	kg/mm^2
% Elongation at Failure	18.12	%

APPENDIX 6082 – T6 EXTRUSION

6082-T6 Extrusion

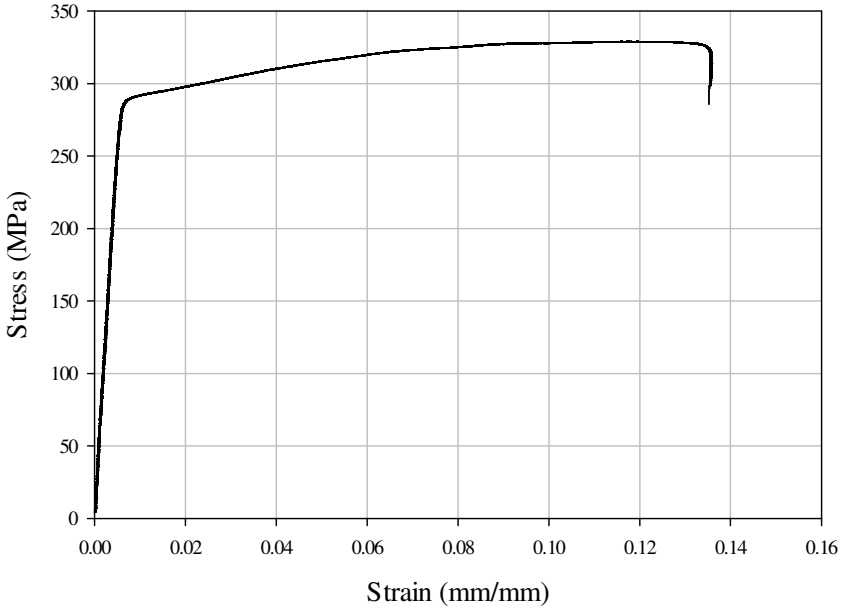

Baseline Zero Time		
Modulus of Elasticity =	51.53	GPa
Yield Stress =	289.40	MPa
Ultimate Tensile Strength =	329.01	MPa
HV_5 =	109.18	kg/mm^2
% Elongation at Failure	13.57	%

6082-T6 Extrusion

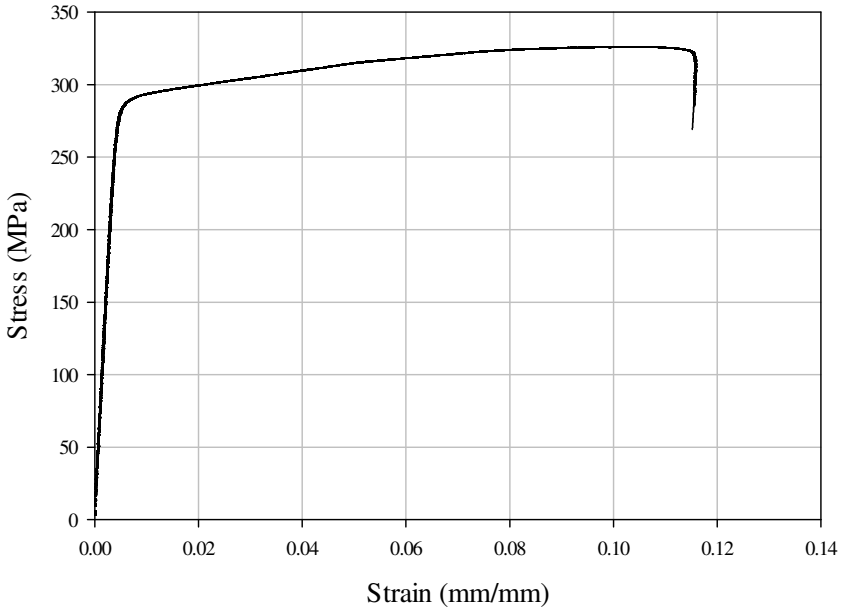

150°C Zero Time		
Modulus of Elasticity =	67.44	GPa
Yield Stress =	288.08	MPa
Ultimate Tensile Strength =	325.97	MPa
HV_5 =	113.29	kg/mm^2
% Elongation at Failure	11.59	%

6082-T6 Extrusion

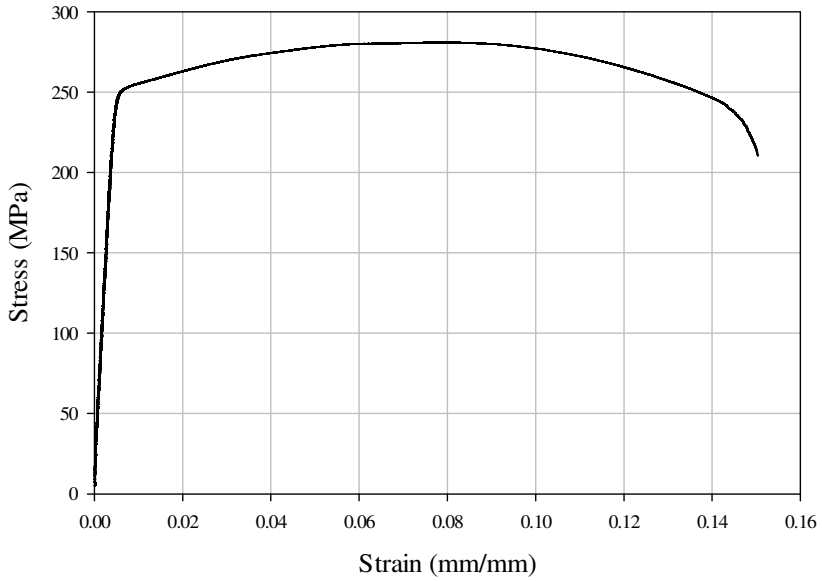

250°C Zero Time		
Modulus of Elasticity =	53.04	GPa
Yield Stress =	252.21	MPa
Ultimate Tensile Strength =	281.02	MPa
HV_5 =	90.53	kg/mm^2
% Elongation at Failure	15.02	%

6082-T6 Extrusion

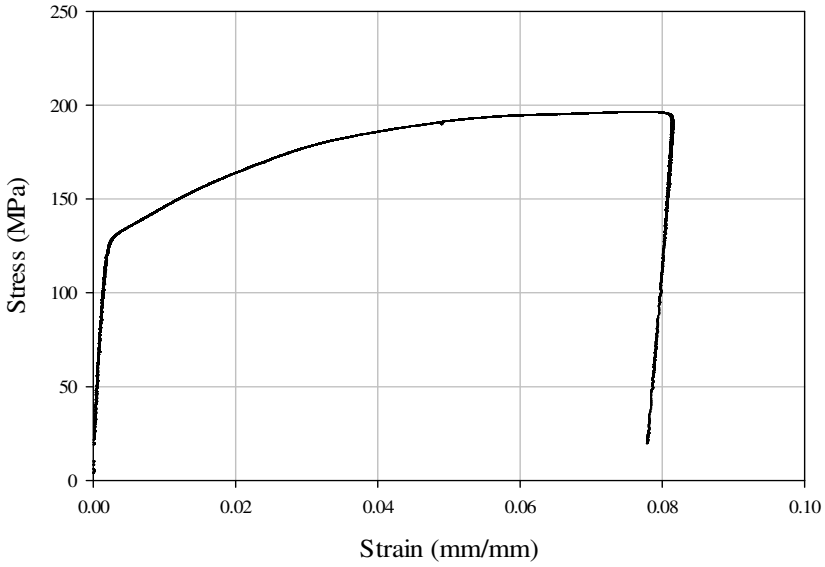

300°C Zero Time		
Modulus of Elasticity =	63.19	GPa
Yield Stress =	133.33	MPa
Ultimate Tensile Strength =	196.45	MPa
HV_5 =	60.87	kg/mm^2
% Elongation at Failure	8.15	%

6082-T6 Extrusion

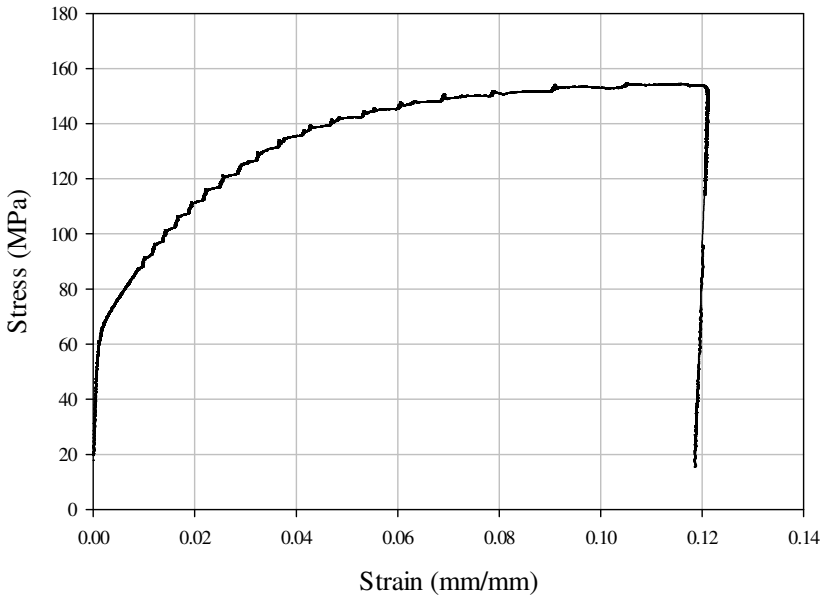

350°C Zero Time		
Modulus of Elasticity =	52.12	GPa
Yield Stress =	72.06	MPa
Ultimate Tensile Strength =	154.85	MPa
HV_5 =	45.40	kg/mm^2
% Elongation at Failure	12.12	%

6082-T6 Extrusion

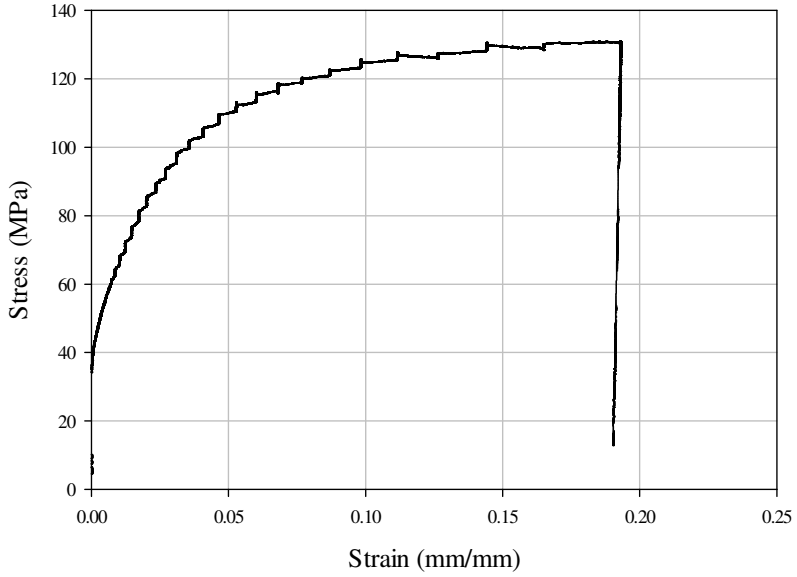

400°C Zero Time		
Modulus of Elasticity =	14.83	GPa
Yield Stress =	57.68	MPa
Ultimate Tensile Strength =	130.98	MPa
HV_5 =	36.96	kg/mm^2
% Elongation at Failure	19.31	%

6082-T6 Extrusion

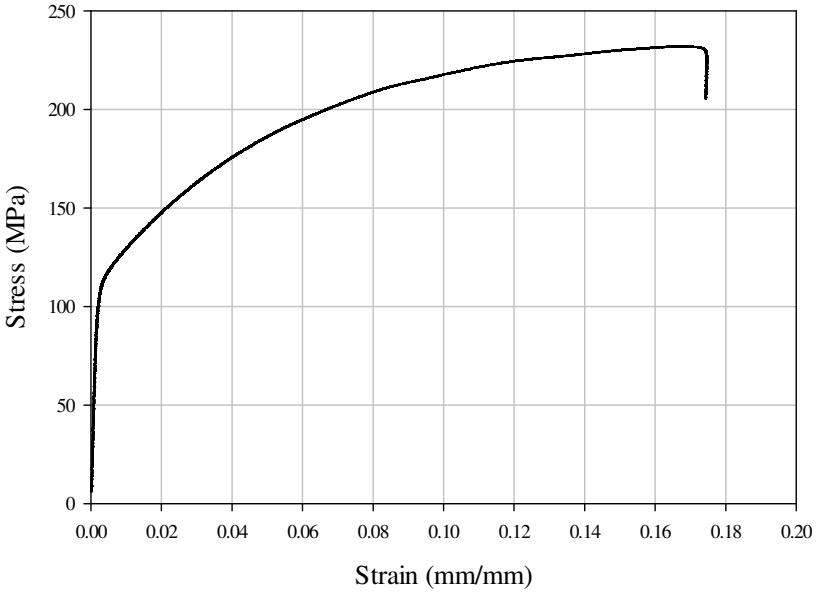

500°C Zero Time		
Modulus of Elasticity =	60.19	GPa
Yield Stress =	114.34	MPa
Ultimate Tensile Strength =	0.00	MPa
HV_5 =	76.21	kg/mm^2
% Elongation at Failure	17.46	%

APPENDIX MATERIAL PROPERTIES

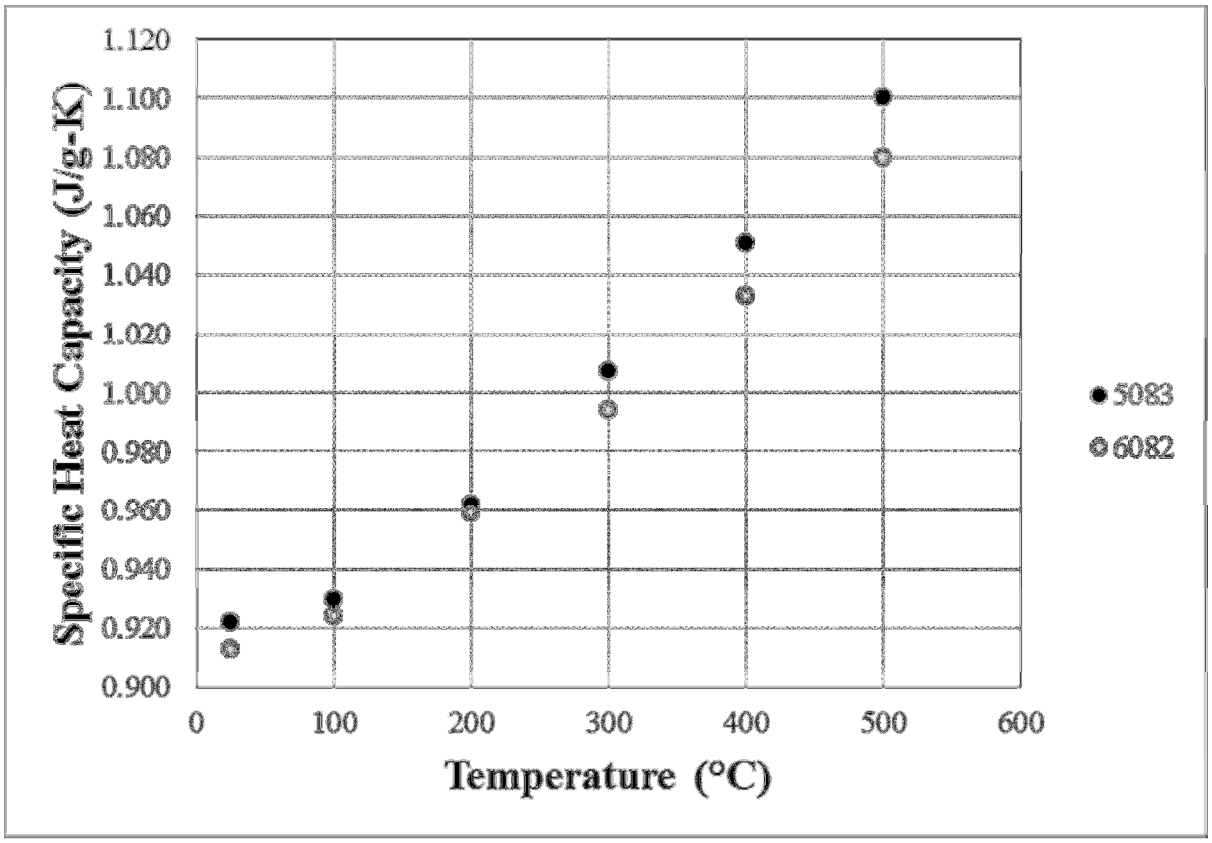
Specific Heat Capacity (J/g-K)
1.120
1.100
1.080
1.060
1.040
1.020
1.000
0.980
0.960
0.940
0.920
0.900
0
100
200
300
400
500
600
Temperature (°C)
5083
6082

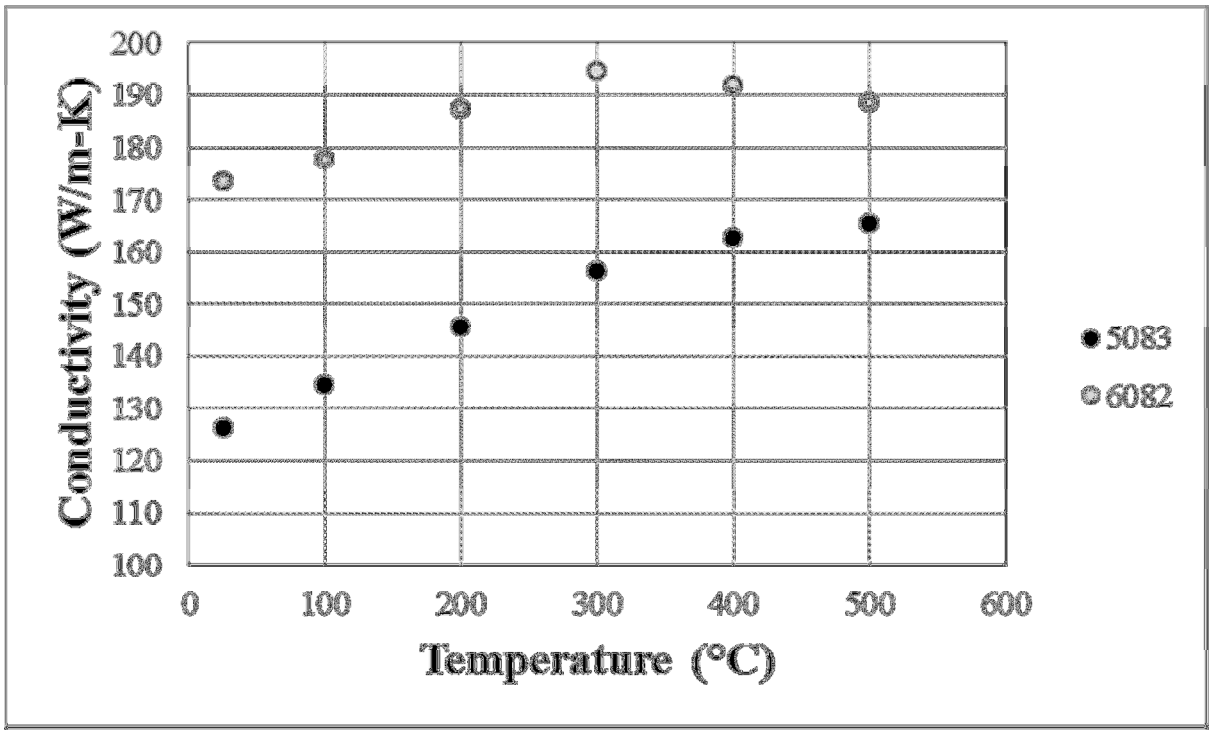
Conductivity (W/m-K)
200
190
180
170
160
150
140
130
120
110
100
0
100
200
300
400
500
600
Temperature (°C)
5083
6082

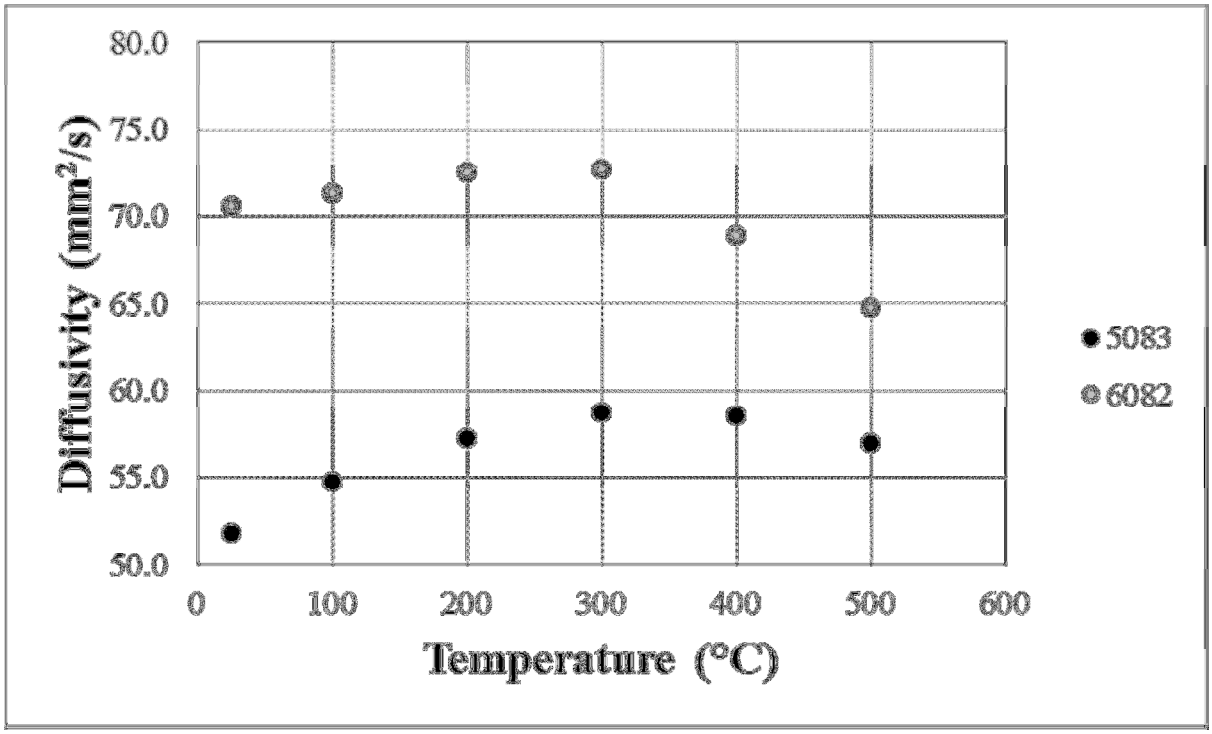
80.0
75.0
70.0
65.0
60.0
55.0
50.0
Diffusivity (mm²/s)
0
100
200
300
400
500
600
Temperature (°C)
5083
6082

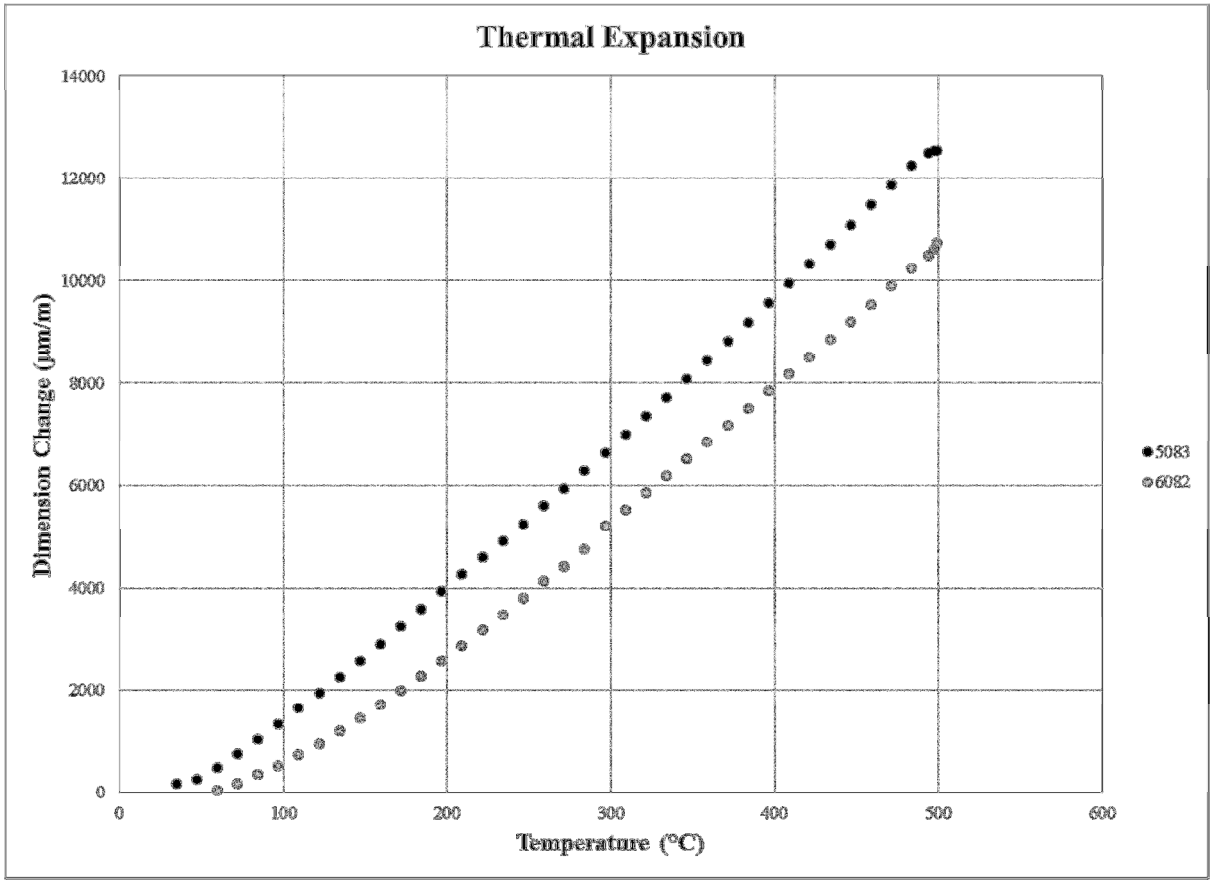
Thermal Expansion
14000
12000
10000
8000
6000
4000
2000
0
Dimension Change (µm/m)
0
100
200
300
400
500
600
Temperature (°C)
5083
6082

Material Properties